Biochemical Pharmacology 218 (2023) 115921

Contents lists available at ScienceDirect

Biochemical Pharmacology

journal homepage: www.elsevier.com/locate/biochempharm

The development of potent, competitive CXCR4 antagonists for the prevention of cancer metastasis

Isabel Hamshaw, Marco M.D. Cominetti, Wing-Yee Lai, Mark Searcey, Anja Mueller *

School of Pharmacy, University of East Anglia, Norwich, UK

ARTICLE INFO

Keywords:
CXCR4
CXCR4 antagonist
CXCL12
Maleimide
Chemokine receptor
Migration

ABSTRACT

Cancer metastasis is the cause of up to 90 % of cancer related mortality. The CXCR4 receptor and its cognate ligand, CXCL12, have major roles in enabling cancer metastasis and consequently, the CXCR4 receptor has become an attractive therapeutic target for the prevention of metastasis. Despite this, CXCR4 antagonists have had limited success in clinical trials due to cellular toxicity and poor stability and efficacy. In this study, we developed a novel, competitive CXCR4 antagonist (IS4) that through copper-catalysed-azide-alkyne-cycloaddition can be clicked to other chemical moieties such as fluorescent dyes (IS4-FAM) for CXCR4-based imaging. We determined that these CXCR4 antagonists were non-toxic and could be used to specifically label the CXCR4 receptor. Furthermore, IS4 and IS4-FAM inhibited CXCL12-stimulated cancer cell migration and Ca^{2+} release in both adherent and suspension cell lines with similar or improved potency as compared to two literature CXCR4 antagonists. Our results highlight the potential of IS4 and IS4-FAM as research tools and as potent CXCR4 antagonists for the prevention of metastasis.

1. Introduction

In 2023 approximately 1.96 million new cancer cases and 0.6 million cancer-related deaths are projected to occur in the US alone with the global cancer burden estimated at 19.3 million new cases and 10 million cancer-related deaths worldwide [1,2]. Of these cancer-related deaths, 66–90% are due to metastasis [3,4].

Small 8–12 kDa peptides called chemokines play a key role in tumour progression and metastasis [5]. Chemokines are signalling molecules that enable the migration of cells along a concentration gradient to sites of infection and injury or to secondary lymphoid organs for maturation [6,7]. Specifically, the binding of the chemokine to its corresponding chemokine receptor leads to conformational changes, which activates downstream signalling pathways that promote migration [8].

CXCL12, and its cognate G protein-coupled receptor, CXCR4, have major roles in neutrophil homeostasis. Briefly, expression levels of CXCR4 increase on old or senescent neutrophils, aiding in their clearance from the blood to the bone marrow due to a CXCL12 gradient [9]. This increased expression or overexpression of CXCR4 has also been detected in more than 30 human cancers including acute myeloid leukaemia, breast, ovarian, melanoma, thyroid, renal, pancreatic, prostate cancer, and salivary gland neoplasms to name a few [10–18]. This makes CXCR4 the most commonly overexpressed chemokine receptor on tumour cells and enables these cells to migrate to tissue sites in the body that naturally express CXCL12 such as the bone marrow, brain, lungs and liver [13,19]. Therefore, the inhibition of the CXCR4/CXCL12 signalling axis can potentially lead to the prevention of CXCR4 driven tumour metastasis and highlights the potential clinical value of CXCR4 antagonists.

To date, the only US Food and Drug Administration approved CXCR4 antagonist is AMD3100 (Plerixafor, Mozobil ®) which is used for autologous stem cell transplantation in patients with multiple myeloma and non-Hodgkin's lymphoma [20]. While there are many CXCL12/CXCR4-based antagonists in pre-clinical trials including CXCR4 antibodies, peptide inhibitors, natural products, small molecule compounds and microRNAs, only a few have entered clinical trials, reviewed in Zhao

Abbreviations: CuAAC, copper-catalysed-azide-alkyne cycloaddition; CXCR4, C-X-C Motif Chemokine Receptor 4; CXCL12, C-X-C Motif Chemokine Ligand 12; DCM, Dichloromethane; DIPEA, N,N-Diisopropylethylamine; DMF, N,N-Dimethylformamide; ECL, Extracellular loop; EDT, Ethane-1,2-dithiol; FAM, Fluorescein amidites; HoBt, 1-Hydroxybenzotriazole; HBTU, 2-(1h-Benzotriazole-1-yl)-1,1,3,3-tetramethyluronium hexafluorophosphate; IC_{50}, half-maximal inhibitory concentration; MALDI-TOF, Matrix-assisted laser desorption/ionization-time of flight; NMP, N-Methyl-2-pyrrolidone; pIC_{50}, negative log of the IC_{50}; TFA, Trifluoroacetic acid; TIPS, Triisopropylsilane.

* Corresponding author.
E-mail address: anja.mueller@uea.ac.uk (A. Mueller).

https://doi.org/10.1016/j.bcp.2023.115921
Received 10 August 2023; Received in revised form 9 November 2023; Accepted 10 November 2023
Available online 11 November 2023

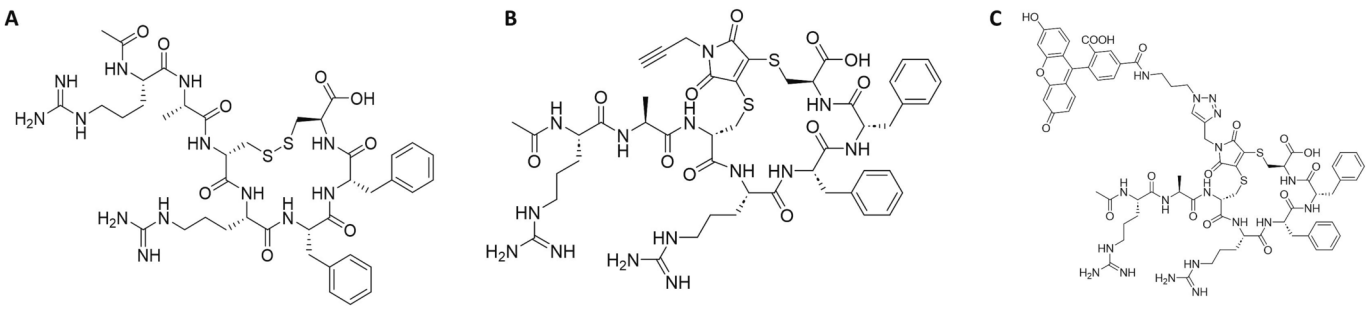

Fig. 1. Structures of peptide 10, IS4 and IS4-FAM. (A) Peptide 10, (B) IS4 and (C) IS4-FAM are CXCL12-derived small cyclic CXCR4 inhibitory peptides. They are seven amino acid peptides Arg-Ala-[DCys-Arg-Phe-Phe-Cys] with the molecular weights of 942.13, 1075.23 and 1533.66, respectively.

et al., [21]. This is due to many CXCR4 antagonists having poor efficacy and/or toxicity [19,22]. Therefore, the development of novel CXCR4 antagonists is paramount for the progression of personalized medicine and cancer therapeutics.

Inspired by the N-terminal sequence of CXCL12, Portella et al., [23] designed a library of cyclic peptides as CXCR4 inhibitors. Subsequent work by Di Maro et al., [24] evaluated a combination of acetylation and the introduction of a D-amino acid. Together with the cyclic nature of the peptide, these modifications led to excellent inhibitory activity and reduced sensitivity to proteases and consequent serum stability of peptide 10 (Fig. 1A) [24]. Introduction of a functionalized maleimide via reaction of cysteine thiols with N-propargyl-2,3-dibromomaleimide (IS4, Fig. 1B) can further increase stability to protease and offer a handle for further selective conjugation of functional elements to a peptide via click chemistry [25].

Copper (I) catalysed-azide-alkyne-cycloaddition (CuAAC) click chemistry reactions are fast, simple to use, easy to purify, versatile and give high product yields. Azide-alkyne based click reactions are particularly convenient and can be introduced into biomolecules without changing their properties or causing cellular toxicity [26]. Therefore, click chemistry has several biomedical applications such as the tagging of therapeutics with fluorescent probes and loading of nanoparticles with drugs for nanoscale drug delivery [27]. Additionally, unlike antibodies, alkyne and azide groups are very small, highly energetic and have narrow reactivity thus, could be used for long term antagonist experimentation [28]. While fluorescent dyes or tags such as biotin could be used instead of 'click' chemistry, these often involve purification and/or multiple wash steps, with excess prelabelled reagents being hard to remove from the tissues and preventing multistep labelling. Therefore, click reactions can potentially reduce background fluorescence as well as reduce the need for multiple wash steps [29].

In this study we developed a novel, serum stable, competitive CXCR4 antagonist (IS4) that through the introduction of a maleimide can be conjugated to other chemical moieties such fluorescent dyes (IS4-FAM, Fig. 1C) for CXCR4-based imaging without introducing cytotoxicity. We then demonstrated that both CXCL12-stimulated cancer cell migration and intracellular Ca^{2+} release can be inhibited by these novel CXCR4 antagonists with similar or improved potency as compared to two literature CXCR4 antagonists: AMD3100 and peptide 10. This highlights the potential of IS4 and IS4-FAM as potent CXCR4 antagonists for the prevention of metastasis and the applicability of future chemical modification through CuAAC.

2. Materials and methods

2.1. Cell culture

The Jurkat (acute T cell leukaemia), Chinese hamster ovary cell (CHO), THP-1 (acute monocytic leukaemia), PC3 (metastatic prostate cancer derived from a grade IV adenocarcinoma in the bone), MCF-7 (metastatic adenocarcinoma derived from mammary glands) and SKMEL-28 (malignant melanoma) cell lines were purchased from ATCC (Teddington, UK) and the vascular smooth muscle cells (VSMC) cells were purchased from Cell Applications Inc. (CA, USA). Jurkat, THP-1, PC3 and SK-MEL-28 cells were grown in 75 cm^3 flasks (ThermoFisher Scientific, Loughborough, UK) and maintained under standard conditions: 37 °C in a 95 %/5% air/CO_2-humidified environment using Roswell Park Memorial Institute (RPMI) medium (Biosera, Nuaille, France) supplemented with 10 % v/v FBS (Invitrogen, Paisley, UK) 2 mM L-glutamine (Invitrogen, Paisley, UK) and 100 μM non-essential amino acids (Gibco, ThermoFisher Scientific, Loughborough, UK). MCF-7, and CHO cells were grown in 75 cm^3 flasks and maintained under standard conditions: 37 °C in a 95 %/5% air/CO_2-humidified using Dulbecco's modified Eagle medium (DMEM) (Biosera, Nuaille, France) with 10 % FBS, 100 μM non-essential amino acids and 2 mM L-glutamine. Adherent cells were sub-cultured at 80–90 % confluency. Suspension cell lines Jurkat and THP-1 were cultured until the cell density reached approximately $1x10^6$ mL $^{-1}$. The VSMCs were grown in 75 cm^3 flasks and maintained as described in [30].

2.2. Literature CXCR4 antagonists

AMD3100 was purchased from Santa Crus Biotechnology (Heidelberg, Germany). The design of peptide 10 is discussed in detail in Di Maro et al.,[24]. All CXCR4 antagonists were dissolved in DMSO (Sigma Aldrich, Hertfordshire, UK) to 100 μM.

2.3. Synthesis of novel CXCR4 antagonists

All reagents and solvents were purchased from Merck (New Jersey, USA), Fluorochem (Glossop, UK), Fisher Scientific (Loughborough, UK) or Cambridge Reagents (Lincolnshire, UK).

Peptides were synthesis on a Syrol II XP using standard Fmoc solid phase peptide synthesis. All structure shown in Fig. 1. Purification and analysis by HPLC are described in the respective paragraph. A purity above 95% was considered the minimum threshold for biology testing. Mass spectrometry analysis to confirm the identity of the compounds was performed via MALDI-TOF (KRATOS AXIMA-CFR or AXIMA Performance) or via LC-MS (service run by Dr Anthony Hinchliffe, UEA Science Analytical Facility). NMR spectra were recorded on a Bruker Ultrashield Plus 400. The chemical shifts for both ^1H and ^{13}C spectra are reported in ppm and referenced to the residual solvent peak. Multiplicities are described as s = singlet, d = 97 doublet, dd = doublet of doublet, t = triplet, q = quartet, m = multiplet and b = broad. Coupling constants are reported in hertz. Data analysis and presentation was performed with Bruker TopSpin 3.5 software. The melting point of IS3 was measured on a Stuart Scientific melting point apparatus SMP3 and were reported uncorrected.

2.3.1. Peptide synthesis

The synthesis was conducted using a H-Cys-(Trt)-2ClTrt resin with 0.63 mmol/g. Batches of 100 mg of resin were swollen by shaking in

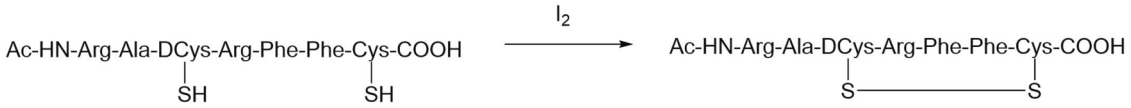

Fig. 2. Formation of a disulphide bond in peptide 10 using iodine.

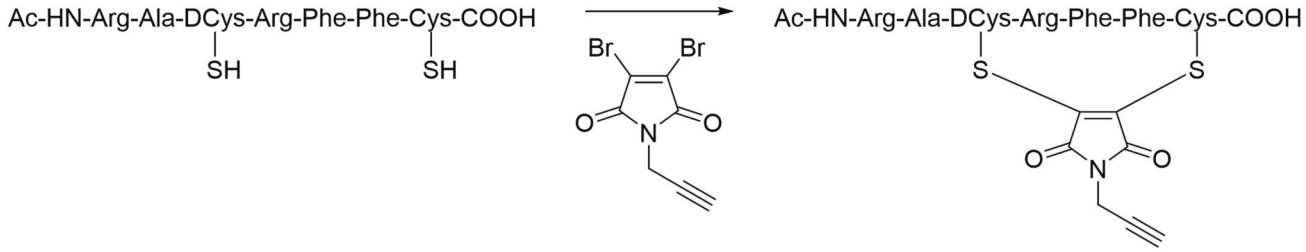

Fig. 3. Synthesis of IS4 by cyclization of peptide 10 using N-propargyl-2,3-dibromomaleimide (IS3).

DCM (~2 mL, 30 min) and subsequently in DMF (~2 mL, 30 min). Each coupling reaction was achieved by subsequent addition of the following reagents to the resin: a 4-fold excess of amino acid (0.5 M in NMP, except arginine – 0.5 M in DMF), a solution of HBTU (0.45 M, 3.9 equivalents) and HOBt (0.45 M, 4 equivalents) in DMF and finally, DIPEA (2 M, 8 equivalents) in NMP. Each coupling was performed twice for 45 min. Deprotection of the Fmoc group was attained by treating the resin with 40 % piperidine in DMF (3 mL, 10 min, 2 times). After completion of the peptide sequence, acetylation of the N-terminal was obtained by shaking the resin for 45 min with a solution of acetyl chloride (4 equivalents) and DIPEA (8 equivalents) in 2 mL of DMF (acetyl chloride was mixed quickly to DMF, followed by DIPEA, mixed for 10 s, and then added to the resin). Completion of the acetylation was assessed by Kaiser Test. If the test proved positive, the acetylation was repeated. The resin was washed with DMF, methanol/DCM 1/1 and DCM prior to drying under vacuum.

2.3.2. Peptide cleavage

The peptide was cleaved and deprotected by shaking the resin with TFA/H_2O/TIPS/EDT (94/2.5/1/2.5 % v/v/v/v) for 3 h (5 mL for 100 mg of resin). The cleavage cocktail was collected, and the resin was washed with fresh TFA, which was added to the previous solution. The solvent was evaporated under reduced pressure and the crude linear peptide was recovered by precipitation and extensively washed with cold diethyl ether to give a powder.

2.3.3. Disulphide bond formation (peptide 10)

The crude peptide from a batch of 100 mg of resin was dissolved in 32 mL of AcOH, and 8 mL of H_2O. Iodine (1 equivalent calculated considering the crude linear peptide as pure) was added, and the mixture was stirred for 1 h at room temperature (RT), Fig. 2. Following this, the solution was diluted with water and any iodine left was extracted from the mixture using chloroform. The aqueous phase was partially evaporated under reduced pressure and the concentrated solution was freeze dried to yield the crude cyclized peptide, peptide 10 (Fig. 1A).

2.3.4. Cyclisation by maleimide stapling (IS4)

Similar to the procedure reported in Grison et al., [25], the crude peptide from a batch of 300 mg of resin was dissolved in water/acetonitrile 9/1 (200 mL) at a concentration of 1.1 mg/mL. While stirring vigorously, a solution of N-propargyl-2,3- dibromomaleimide (referred to as IS3) in acetonitrile was added slowly to IS4 (1 equivalent to the theoretical peptide, 20 mL of acetonitrile), Fig. 3. The resulting solution was stirred under nitrogen for 16 h at room temperature. The volume was reduced by evaporation under reduced pressure and the remaining solvent was freeze dried. The yellow solid obtained was triturated with ethyl acetate, dried under reduced pressure, and purified by preparative HPLC (yield 16 %).

2.3.5. Fluorophore addition via CuAAC (IS4-FAM)

Purified IS4 (11.53 mg) was dissolved in 50 μL of DMF followed by FAM azide, 5-isomer (Abcam product: ab146476, 5 mg), $Cu(MeCN)_4PF_6$ (1 mg) and DIPEA (3.8 μL), Fig. 4. After stirring for 16 h at room temperature the solution was purified as described in the following paragraph. All these procedures were performed while minimizing exposure to light.

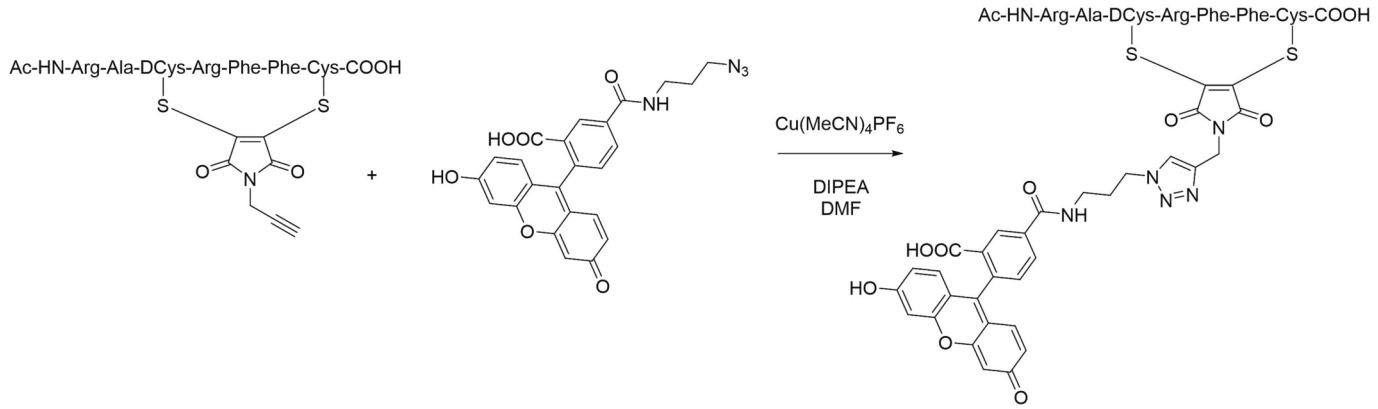

Fig. 4. Conjugation of FAM azide to IS4.

2.3.6. Purification and analysis

Peptides were purified by preparative HPLC using an Agilent Technologies 1260 Infinity Series equipped with an Agilent ZORBAX XDB-C18 21.2 mm × 150 mm column (5 μm pore size). Separation was obtained with a linear gradient from 5 % to 95 % of methanol in water over 15 min followed by 5 min of 95 % methanol and a 3-minute gradient to return to the initial conditions (flow rate of 20 mL/min, all solvents contain 0.05 % TFA).

Peptides were analysed by analytical HPLC using an Agilent Technologies 1200 Series HPLC equipped with an Agilent ZORBAX Eclipse YDB-C18 4.6 mm x 150 mm column (5 μM pore size). Samples were eluted using a linear gradient from 5 % to 95 % of methanol in water over 15 min followed by 5 min of 95 % methanol and a 5-minute gradient to return to the initial conditions (flow rate of 1.0 mL/min, all solvents contain 0.05 % TFA). The UV detector was set to record at 254 and 210 nm wavelengths. Integration of the traces was used to assess purity. Only samples with purity ≥ 95 % were considered for biological evaluation.

Molecular weights of compounds were confirmed by MALDI-TOF on a KRATOS AXIMA-CFR using either sinapinic acid or alpha-cyano-4-hydroxycinnamic acid as matrix.

2.4. Immunofluorescence (IF) microscopy

2.4.1. CXCR4 expression

MCF-7, PC3 and SKMEL-28 cells were seeded onto ethanol sterilized 0.13 mm glass cover slides in a 12-well plate at a density of 0.5 x10^5 to 1.5x10^5 mL^{-1} in either DMEM or RPMI 1640 media for 24 h at 37 °C in a 95 %/5% air/CO_2-humidified environment. Cells were washed twice in ice-cold 1X PBS (ThermoFisher Scientific, Loughborough, UK) and fixed with 4 % paraformaldehyde (ThermoFisher Scientific, Loughborough, UK) for 10 min. Cells were washed twice in ice-cold 1X PBS then incubated with 1:200 primary mouse 12G5 anti-CXCR4 (sc-12764, Santa Cruz Biotechnology, Heidelberg, Germany) for 1 h at 4 °C.For negative control, no primary antibody was added. Cells were washed twice in ice-cold 1X PBS then incubated with 1:200 secondary goat anti-mouse IgG Alexa Fluor® 488 antibody (Abcam, Cambridge, UK) for 1 h at 4 °C. Cells were washed twice in ice-cold 1X PBS then incubated with DAPI (Sigma Aldrich, Hertfordshire, UK) for 10 min at 4 °C. Cells were washed twice in ice-cold 1X PBS and finally the cover slides were mounted onto glass slides using DPX mountant (ThermoFisher Scientific, Loughborough, UK).

THP-1 and Jurkat cells were harvested, centrifuged then resuspended in ice-cold 1X PBS at a density of 1x10^6 mL^{-1} whereupon the above procedure was conducted with washing occurring by centrifugation and resuspension in 1X PBS. Finally, 10 μL of cell solution was pipetted into DPX mountant and a cover slide affix on top. Cells were visualized for CXCR4 expression using a Leica DMIL LED inverted microscope using a 63x objective with an overall magnification of 35x.

2.4.2. Orthosteric site identification

Methodology as above; however, the relevant antagonists were added to the plate for 1 h at 37 ℃ prior to washing and fixed with 4 % paraformaldehyde. Cells were then incubated with either 1:200 of anti-CXCR4 (12G5) or 1:200 anti-CXCR4 (4G10, sc-53534, Santa Cruz Biotechnology, Heidelberg, Germany) for 1 h at 4 °C before resuming above methodology.

2.5. Confocal microscopy

MCF-7 cells were seeded onto ethanol sterilized 0.13 mm glass cover slides in a 12-well plate at a density of 1 x10^5 mL^{-1} in DMEM media for 24 h at 37 °C in a 95 %/5% air/CO_2-humidified environment. Cells were washed twice in ice-cold 1X PBS then incubated with 1:200 primary mouse 4G10 anti-CXCR4 for 1 h at 4 °C and 1 μM IS4-FAM. For negative control, no primary antibody was added. Cells were washed twice in ice-cold 1X PBS then incubated with 1:200 secondary goat anti-mouse IgG Alexa Fluor® 568 antibody (Abcam, Cambridge, UK) for 1 h at 4 °C. Cells were washed twice in ice-cold 1X PBS then incubated with DAPI for 10 min at 4 °C. Cells were washed twice in ice-cold 1X PBS and finally the cover slides were mounted onto glass slides using DPX mountant.

Jurkat cells were harvested, centrifuged then resuspended in ice-cold 1X PBS at a density of 1x10^6 mL^{-1} whereupon the above procedure was conducted with washing occurring by centrifugation and resuspension in 1X PBS. Finally, 10 μL of cell solution was pipetted into DPX mountant and a cover slide affix on top.

All slides were then imaged using a Zeiss LSM 980-Airyscan 2 confocal laser scanning microscope. Super-resolution Z-stacks images were taken at 0.15 μm intervals to allow for selection of precise focal planes, acquired using Zen 3.1 (Blue) with a 100x objective.

2.6. Flow cytometry

Cells were harvested at a density of 1x10^6 mL^{-1} in 0.5 % bovine serum albumin (BSA)/PBS (ThermoFisher Scientific, Loughborough, UK). Cells were washed twice in ice-cold 1X PBS then incubated with 1:200 anti-CXCR4 (12G5) or 1:50 anti-CXCR7/ACKR3 (11G8, R&D Systems, Abingdon, UK) for 1 h at 4 °C. A mouse IgG isotype control (ThermoFisher Scientific. Loughborough, UK) was used to validate the use of goat anti-mouse secondary Alexa Fluor® 488 only as a negative control and background staining was found to be negligible. Therefore, for all future negative controls, no isotype control was added. Cells were washed twice in ice-cold 1X PBS then incubated with 1:200 secondary goat anti-mouse Alexa Fluor® 488 for 1 h at 4 °C. Cells were washed twice in ice-cold 1X PBS then analysed using a CytoFLEX (Beckman Coulter) with CytExpert (v2.4) software.

Data analysis: Fluorescent intensity values were measured with a blue 488 nm laser using the FITC channel. The cell population were plotted as forward scatter-area (FSC-A) verses side scatter-area (SSC-A) to gate out any perturbations and as FSC-A verses forward scatter-height (FSC-H) to gate only singlet events. Cells were gated to 10,000 events and median fluorescence-area (MFI) was recorded for each sample. Relative fluorescence was calculated as; MFI sample/ MFI negative control then plotted using GraphPad Prism 8 software.

2.7. Cell viability assay

CellTiter 96® AQ_{ueous} One Solution Cell Proliferation Assay (Promega, Southampton, UK) containing a tetrazolium compound [3-(4,5-dimethylthiazol-2-yl)-5-(3-carboxymethoxyphenyl)-2-(4-sulfophenyl)–2H-tetrazolium, inner salt; MTS] was used to determine cell viability. 100 μL of cells were seeded at 1-5x10^5 mL^{-1} into clear 96-well plates. Cells were challenged with 1 μM to 100 μM of CXCR4 antagonist and incubated for 72 h at 37 °C in a 95 %/5% air/CO_2-humidified environment. 10 μL of MTS reagent was added to each well and incubated for 4 h at 37 °C in a 95 %/5% air/CO_2-humidified environment. A FLUOstar Optima Fluorometer using Optima software (BMG Labtech) was used at an absorbance of 490 nm to detect the quantity of the coloured formazan product.

Data analysis: Triplicates of each condition were conducted. Percentage survival was calculated as; (average absorbance of sample/ average absorbance of positive control) x 100 and plotted using GraphPad Prism 8 software.

2.8. Intracellular Ca^{2+} release assay

Cells were harvested, centrifuged, and washed twice with calcium flux buffer (137 mM NaCl, 5 mM KCl, 1 mM $MgCl_2$, 1.5 mM $CaCl_2$, 10 mM Hepes, 25 mM D-Glucose, 500 mL purified water; pH 7.4 (all purchased from ThermoFisher Scientific (Loughborough, UK)) before being re-suspended at 2x10^6 mL^{-1}. Cells were incubated with 1 μM CXCR4 antagonist, loaded with 4 μM Fura-2 AM dye (Invitrogen, Paisley, UK)

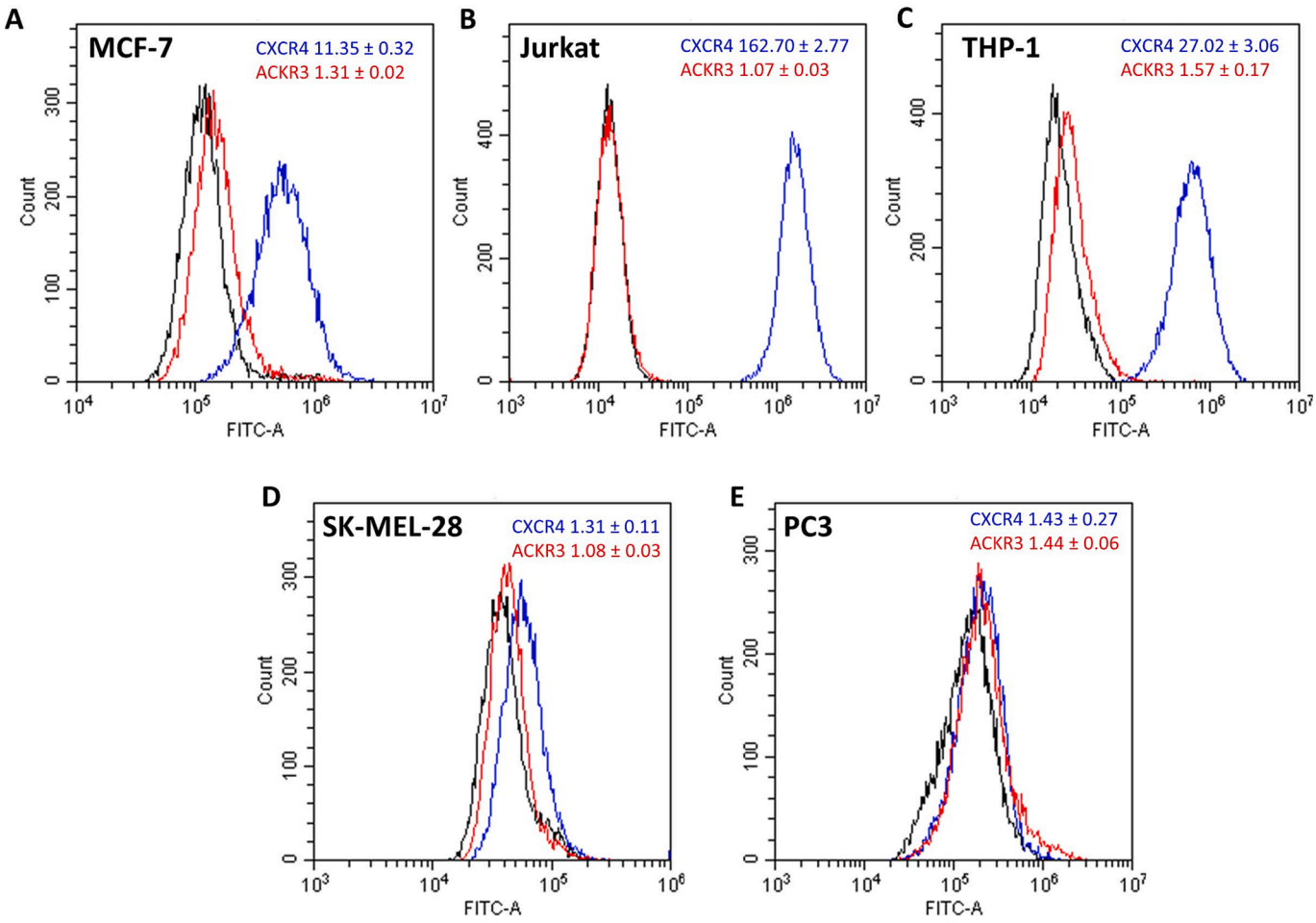

Fig. 5. Expression of CXCR4 and ACKR3 in five cell lines. Representative histogram of CXCR4 (blue) and ACKR3 (red) expression in A) MCF-7, B) Jurkat, C) THP-1, D) SK-MEL-28 and E) PC3 cells as compared to negative control (black). Fluorescent intensity values were measured with a blue 488 nm laser, FITC channel using FITC median fluorescence area (MFI). Relative expression displayed calculated as MFI sample/ MFI negative control. Data are mean ± SD, N = 3–4.

and incubated for 30 min at 37C, air 95 % and 5 % CO_2. After incubation, cells were centrifuged at 1200 rpm for 5 min and washed twice with calcium flux buffer. Finally, 100 μL of cells were loaded into an opaque, black 96-well plate (ThermoFisher Scientific, Loughborough, UK). This plate was loaded into a BMG LabTech FLUOstar Optima Fluorometer programmed to inject 15–50 nM of CXCL12 (Peprotech, London, UK) directly into the 96-well plate after 15 s of recording. Fluorescence was recorded every second for a total recording time of 70 s. Changes in the release of calcium was analysed via ratiometric analyses of the changes in fluorescence at a fixed emission frequency of 510 nm. Using Optima software, data was recorded and analysed as a ratio of 340/380 nm which is directly related to the amount of intracellular calcium release.

Data analysis: Data was expressed as a change in fluorescence ratio (340 nm/380 nm) where the basal fluorescence prior to the addition of chemokine is subtracted from peak fluorescence following addition of chemokine.

2.9. Stability assay

CXCR4 antagonists were incubated in FBS for 30 min at 37 °C in a 95 %/5% air/CO_2 humidified environment before conducting intracellular Ca^{2+} release assays as previously described.

2.10. Chemotaxis assay

The effect of CXCR4 antagonists upon CXCL12 induced migration in suspension cells was observed using ChemoTX 5 μM pore transwell chemotaxis plates (Neuroprobe Inc, Maryland, USA). Wells were blocked with 31 μL of serum free RPMI 1640 containing 1 % BSA for 30 min at room temperature. Media was removed and replaced with 31 μL of 1 nM CXCL12 for Jurkat cells or 5 nM chemokine (all chemokines purchased from Peprotech, London, UK) for THP-1 cells diluted in serum free RPMI 1640 containing 0.1 % BSA. Serum free RPMI 1640 containing 0.1 % BSA was used as a negative control. The 5 μM pore polyvinylprollidone-free polycarbonate membrane was then attached. Jurkat cells were harvested at a concentration of $25x10^4$ mL^{-1} and THP-1 cells at a concentration of $50x10^4$ mL^{-1} in serum free RPMI 1640 containing 0.1 % BSA. Cells were challenged with half log incremental concentrations of CXCR4 antagonist (0.01 nM to 1 μM) and incubated for 30 min at 37 °C in a 95 %/5% air/CO_2-humidified environment. Cells were washed and resuspended in serum free RPMI 1640 containing 0.1 % BSA and 20 μL of cells were loaded onto the surface of the 5 μM pore membrane. The plate was placed inside a humidified chamber and incubated for 4 h at 37 °C in a 95 %/5% air/CO_2-humidified environment. The filter was then removed, and 10 μL of cells were counted from each lower chamber using a hemocytometer to determine the number of cells that had migrated towards the chemokine.

Data analysis: Duplicates of each condition were conducted. The number of migrating cells per condition was counted then averaged) before plotting in GraphPad Prism 8 software.

2.11. Time lapse microscopy

The effect of CXCR4 antagonist upon CXCL12 stimulated migration in adherent cells was observed using time-lapse microscopy. PC3 and SK-MEL-28 cells were harvested at $0.4x10^4$ mL^{-1} cells and seeded into 48-well plates in RPMI 1640 for 24 h at 37 °C in a 95 %/5% air/CO_2-humidified environment. The following day, cells were washed with 1X PBS and resuspended in serum-free RPMI 1640. Cells were challenged by half log incremental concentrations of CXCR4 antagonist (300 pM to 10 μM) in the presence and absence of 10 nM CXCL12. The 48 well plate was inserted into a controlled chamber at 37 °C in a 95 %/5% air/CO_2-humidified environment and time lapse images were taken using a 10x objective on a Zeiss Axio Observer 7 Inverted LED fluorescence motorized microscope with images captured every 5 min for 10 h (120 frames) using Zen-Lite v3-1 (Zeiss).

Data analysis: Using ImageJ software, any shift in the plate over time was corrected using Plugin, Registration, Linear stack alignment with SIFT. 10 cells per condition were manually tracked by clicking on the centre of the cell nuclei throughout consecutive frames. Average cell speed for each sample was calculated as migratory distance/time then averaged over 10 cells and plotted using GraphPad Prism 8 software. Exclusion criteria included cells that died, divided, or left the visual frame.

2.12. Saturation binding

Jurkat and MCF-7 cells were harvested at a density of $1x10^6$ mL^{-1} in 0.5 % BSA/PBS. Cells were washed twice in ice-cold 1X PBS then incubated with half log concentration of IS4-FAM (10 nM to 300 μM) for 1 h at room temperature in the dark. For negative control, no IS4-FAM was added. Cells were washed twice in ice-cold 1X PBS then analysed using a CytoFLEX (Beckman Coulter) with CytExpert (v2.4) software.

Data analysis: Fluorescent intensity values were measured with a blue 488 nm laser using the FITC channel. The cell population were plotted as forward scatter-area (FSC-A) verses side scatter-area (SSC-A) to gate out any perturbations and as FSC-A verses forward scatter-height (FSC-H) to gate only singlet events. Cells were gated to 10,000 events and median fluorescence-area (MFI) was recorded for each sample. Relative fluorescence was calculated as; MFI sample/ MFI negative control then plotted using GraphPad Prism 8 software.

2.13. Competition binding

Jurkat and MCF-7 cells were harvested at a density of $1x10^6$ mL^{-1} in 0.5 % BSA/PBS. Cells were washed twice in ice-cold 1X PBS then incubated with half log concentration of IS4-FAM (10 nM to 300 μM) and 1–10 μM of IS4 for 1 h at room temperature in the dark. For negative control, only IS4 was added. Cells were washed twice in ice-cold 1X PBS then analysed using a CytoFLEX (Beckman Coulter) with CytExpert (v2.4) software.

Data analysis: As previous.

3. Results

Prior to detailed studies of CXC receptor migration, the receptor profiles of several cancer cell lines were characterized. This determined that five cell lines; Jurkat, THP-1, MCF-7, SK-MEL-28 and PC3 cells expressed detectable levels of CXCR4 using immunofluorescence (data not shown) then validated via flow cytometry in comparison to a second CXCL12-binding chemokine receptor; ACKR3 (Fig. 5).

3.1. IS4 binding to CXCR4 is similar to the binding of the CXCL12 mimetic compounds AMD3100 and peptide 10 to CXCR4

To determine if the novel compound IS4 is a CXCL12 mimetic compound, two anti-CXCR4 monoclonal antibodies (mAb) 12G5 and 4G10 were utilized. The conformation-dependent mAb 12G5 recognizes determinants in extracellular loop (ECL) 1 and ECL2 of CXCR4, specifically binding to the E3 epitope in ECL2 [31,32]. This 12G5-CXCR4 binding is like that of CXCL12-CXCR4 binding whereby CXCL12 binds to Asp^{187} and Asp^{262} in the ECL2 of CXCR4 [33]. Therefore, 12G5 and CXCL12 competitively bind CXCR4 [34–36]. Alternatively, the 4G10 CXCR4 mAb recognizing determinants in the N-terminus of CXCR4, specifically the E2 and I6 residues and therefore does not compete with CXCL12 [37].

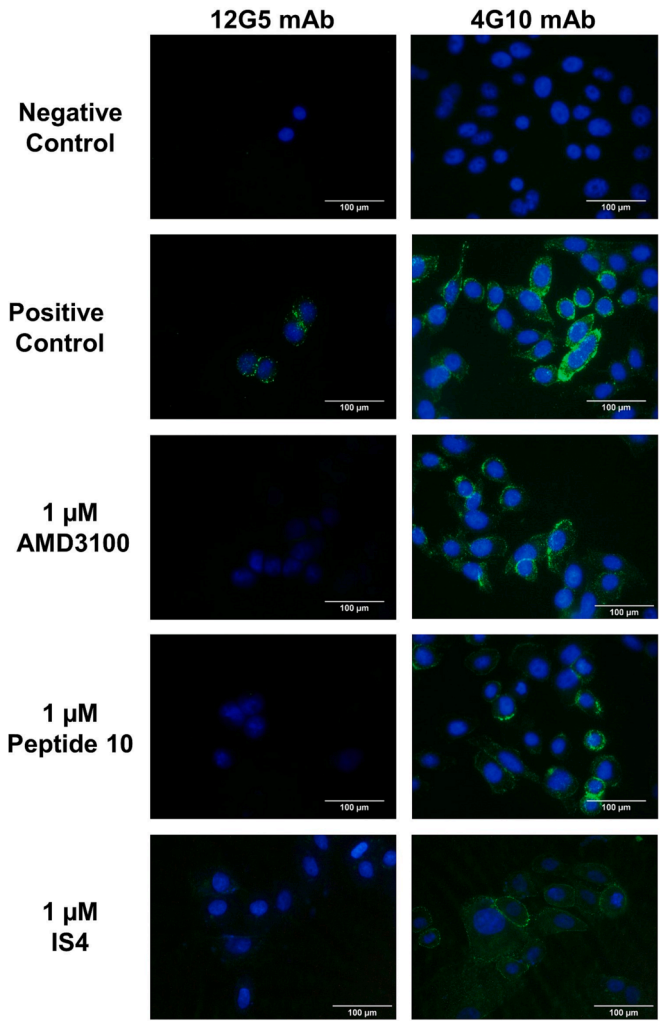

Fig. 6. IS4 binding to CXCR4 is similar to the binding of the CXCL12 mimetic compounds AMD3100 and peptide 10 to CXCR4. Immunofluorescence microscopy of MCF-7 breast cancer cells shows positive expression of CXCR4 (green), visualized using either 12G5 mouse anti-CXCR4 monoclonal antibody (mAb) (binds to the extracellular loops 1 and 2 of CXCR4) or 4G10 mouse anti-CXCR4 mAb (binds to the N-terminus of CXCR4), plus secondary anti-mouse Alexa Fluor® 488 with nuclei indicated by DAPI staining (blue). No antagonist was used for positive controls. Negative control visualized using secondary anti-mouse Alexa Fluor® 488 and DAPI staining only. The CXCL12 mimetic compounds AMD3100 and peptide 10 bind to similar residues on CXCR4 as compared to 12G5 therefore, in the presence of these compounds, fluorescence is lost. Fluorescence is restored with use of the 4G10 anti-CXCR4 mAb in place of 12G5. Data shows representative images from N = 4 acquired with Leica imaging suite using a 63x objective.

AMD3100 is a symmetric bicyclam non-peptide antagonist of CXCR4 that binds acid residues Asp^{171}, Asp^{262} and Glu^{288} in the main ligand binding pocket [38–41]. This is similar to the binding of CXCL12 to CXCR4 whereby salt bridges form between the N-terminal amine of the chemokine and CXCR4 Asp^{97}, the side chain of CXCL12 Lys^1 and CXCR4

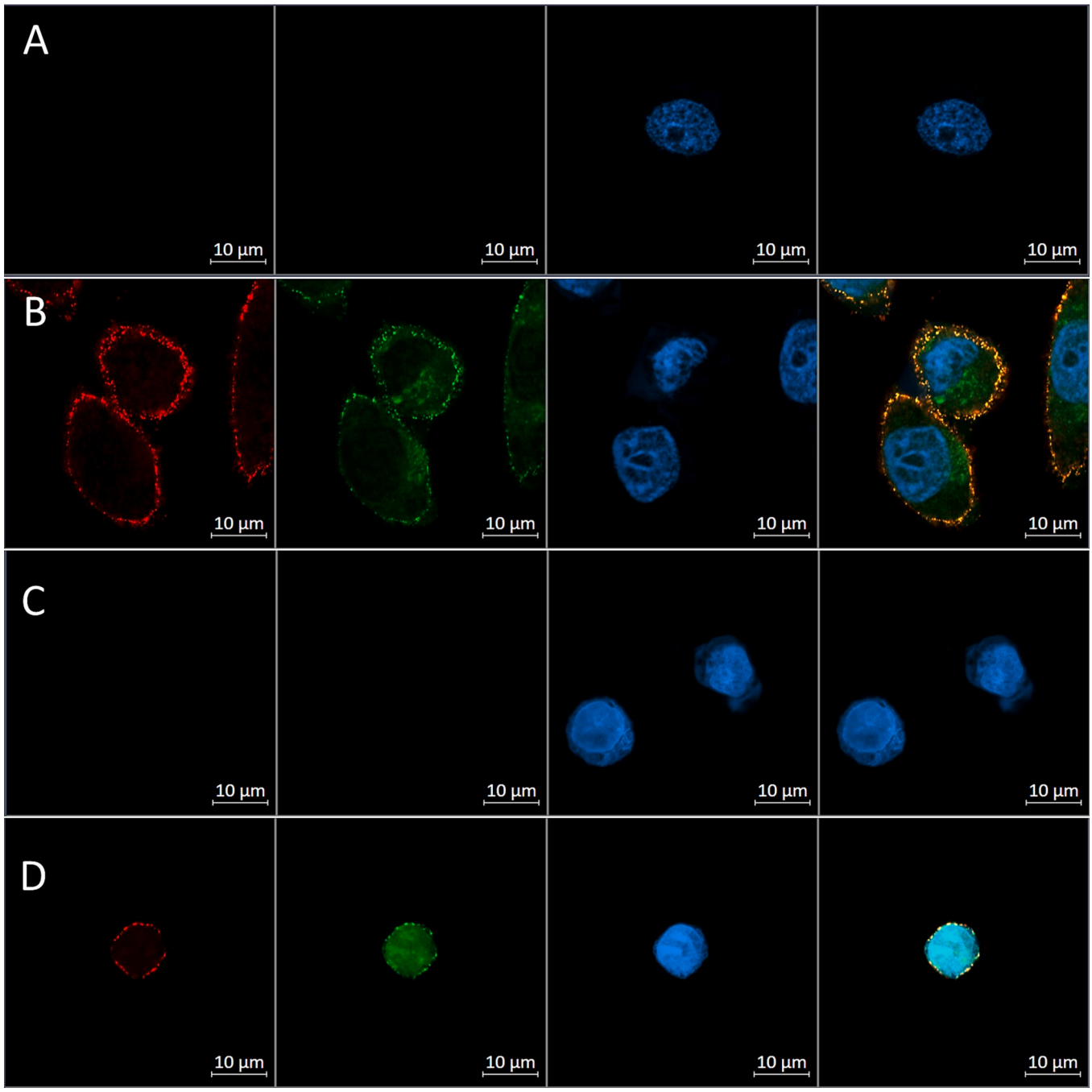

Fig. 7. CXCR4 expression in MCF-7 breast cancer cells and acute T leukemic (Jurkat) cells labelled using mouse anti-CXCR4 antibody (4G10) and 1 µM IS4-FAM. Confocal images of a central Z-stack of A) MCF-7 cells visualized using secondary anti-mouse Alexa Fluor® 568 (red) and DAPI (blue). B) 1:200 anti-CXCR4 (4G10) with secondary anti-mouse Alexa Fluor® 568 (red), 1 µM IS4-FAM (green) and DAPI (blue). C) Jurkat cells visualized using secondary anti-mouse Alexa Fluor® 568 (red)and DAPI (blue). D) 1:200 anti-CXCR4 (4G10) with secondary anti-mouse Alexa Fluor® 568, 1 µM IS4-FAM (green) and DAPI (blue). Data shows representative images from 3 independent experiments with similar findings. Confocal images acquired using Zen 3.1 (Blue) with a 100X objective.

Glu^{288} and CXCL12 Arg^{8} to CXCR4 Asp^{262} [33]. Therefore, AMD3100 functions as a CXCL12 mimetic compound. Furthermore, the novel peptide 10 was also found to be a CXCL12 mimetic compound whereby the Arg^{1} and Arg^{4} residues in peptide 10 makes salt bridges with Asp^{187} and Asp^{97}, respectively and the Phe^{6} resides in peptide 10 forms a hydrogen bond with Glu^{288}[24].

MCF-7 breast cancer cells were incubated with 1 µM of AMD3100 to achieve ~ 99.8 % CXCR4 receptor occupancy and compared to equivalent concentrations of peptide 10 and IS4 [42,43].

Results from these experiments confirmed that AMD3100, peptide 10 and the novel CXCR4 antagonist IS4 all prevented the binding of 12G5 (no visible immunofluorescence) when cells were incubated with these compounds plus 12G5 and the secondary antibody (Fig. 6) [44,45]. However, when using the compounds in the presence of the conformation-independent anti-CXCR4 mAb 4G10, directed against the N-terminal domain of CXCR4, fluorescence was observable and comparable to the positive control [31,32,46].

3.2. *IS4-FAM can directly label CXCR4*

Through CuAAC, IS4 can be clicked to the commercially available fluorescent dye FAM azide, 5-isomer forming IS4-FAM. High

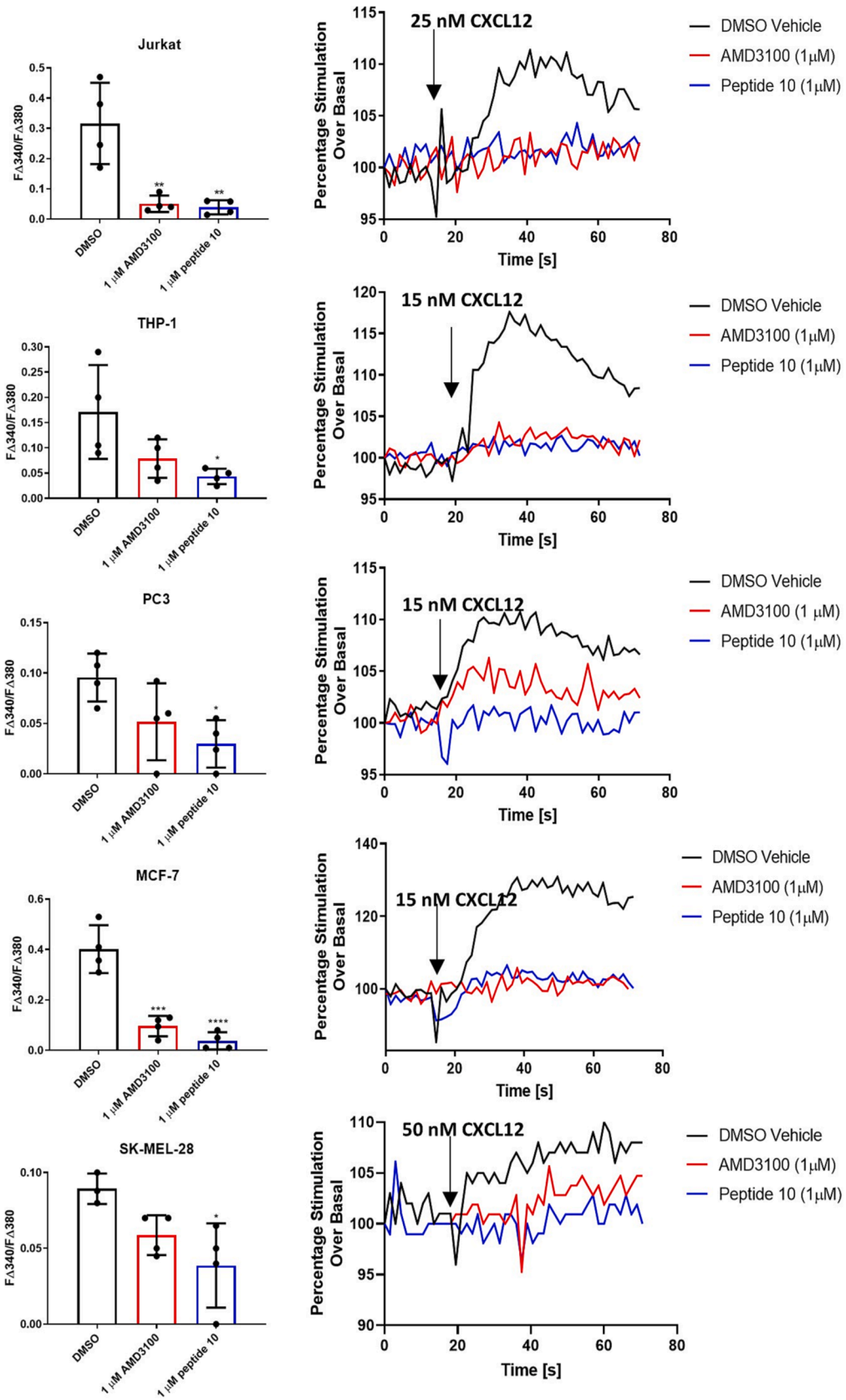

(caption on next page)

Fig. 8. Inhibition of intracellular calcium release in Jurkat, THP-1, PC3, MCF-7 and SK-MEL-28 cells lines by selected literature CXCR4 antagonists. All cell lines were treated with 1 μM CXCR4 antagonist or vehicle equivalent then induced with 25 nM CXCL12 (Jurkat), 15 nM CXCL12 (THP-1, PC3 and MCF-7) or 50 nM CXCL12 (SK-MEL-28). Data is expressed as a change in fluorescence ratio (340 nm/380 nm) where the basal fluorescence prior to the addition of CXCL12 is subtracted from peak fluorescence following addition of CXCL12. Representative traces of each cell line demonstrate percentage change over basal fluorescence when stimulated by chemokine injected after 15 s. Data are mean ± SD, N = 4, One-Way ANOVA and post hoc Dunnett's multiple comparison test comparing conditions to DMSO vehicle equivalent $*p < 0.05$, $**p < 0.01$, $***p < 0.01$ and $****p < 0.001$. Outliers removed by Grubbs (Alpha = 0.05).

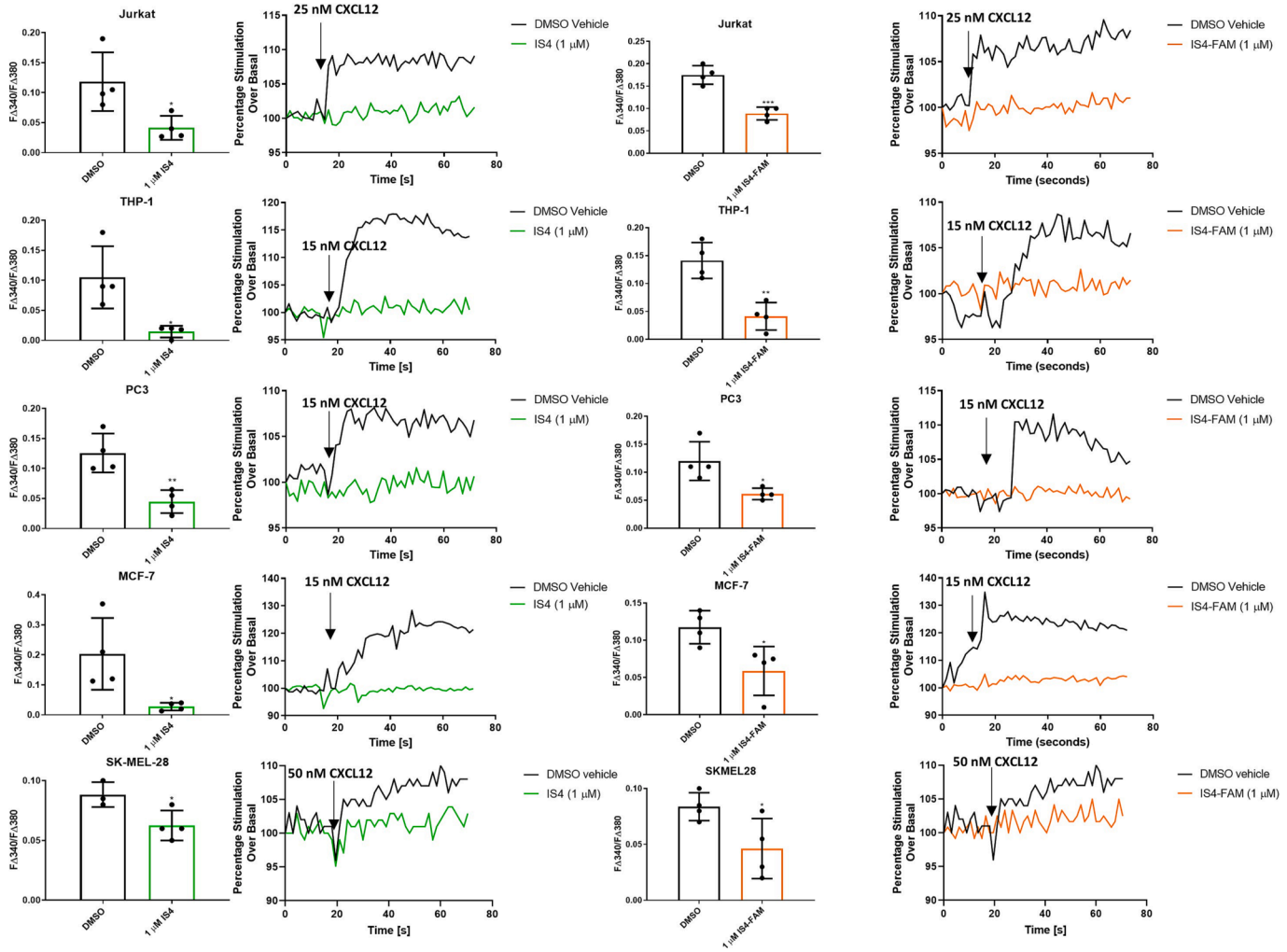

Fig. 9. Inhibition of intracellular calcium release in Jurkat, THP-1, PC3, MCF-7 and SK-MEL-28 cells lines by novel CXCR4 antagonists. All cell lines were treated with 1 μM CXCR4 antagonist or vehicle equivalent then induced with 25 nM CXCL12 (Jurkat), 15 nM CXCL12 (THP-1, PC3 and MCF-7) or 50 nM CXCL12 (SK-MEL-28). Data is expressed as a change in fluorescence ratio (340 nm/380 nm) where the basal fluorescence prior to the addition of CXCL12 is subtracted from peak fluorescence following addition of CXCL12. Representative traces of each cell line demonstrate percentage change over basal fluorescence when stimulated by chemokine injected after 15 s. Data are mean ± SD, N = 4, One-Way ANOVA and post hoc Dunnett's multiple comparison test comparing conditions to DMSO vehicle equivalent $*p < 0.05$ and $**p < 0.01$. Outliers removed by Grubbs (Alpha = 0.05).

concentration IS4-FAM (10 μM) was used to label both MCF-7 and Jurkat cells (Fig. 7). To confirm that the fluorescence seen was due to labelling on the extracellular surface of cells, Z-stacks were created via confocal microscopy and a central cross-section of the cell was taken and compared to 12G5 anti-CXCR4 mAb binding. This demonstrated that IS4-FAM was binding extracellularly with limited internalization.

3.3. IS4 and IS4-FAM inhibit CXCL12-induced Ca^{2+} release in five CXCR4 expressing cancer cell lines

CXCR4 receptor activation can be quantified from changes in downstream secondary messengers such as calcium ions (Ca^{2+}) [47,48]. Therefore, the activity of the two literature CXCR4 antagonists (AMD3100 and peptide 10) and our two novel CXCR4 antagonists (IS4 and IS4-FAM) were evaluated in a fluorescent ratiometric assay, detecting free and bound Ca^{2+}. Fura-2 AM loaded cells were incubated with 1 μM of CXCR4 antagonist or a DMSO vehicle equivalent then injected with 15 nM (THP-1, PC3, MCF-7), 25 nM (Jurkat) or 50 nM (SK-MEL-28) CXCL12 to determine the effect on CXCL12-induced intracellular Ca^{2+} release. While AMD3100 only significantly decreased Ca^{2+} release in Jurkat and MCF-7 cells, peptide 10, IS4 and IS4-FAM significantly decreased Ca^{2+} release in all five cell lines (Figs. 8 and 9).

3.4. IS4 and IS4-FAM inhibit CXCL12-induced migration in suspension cells (Jurkat and THP-1)

To evaluate the capacity of the CXCR4 antagonists to compete with the natural chemokine ligand CXCL12 for interaction with CXCR4,

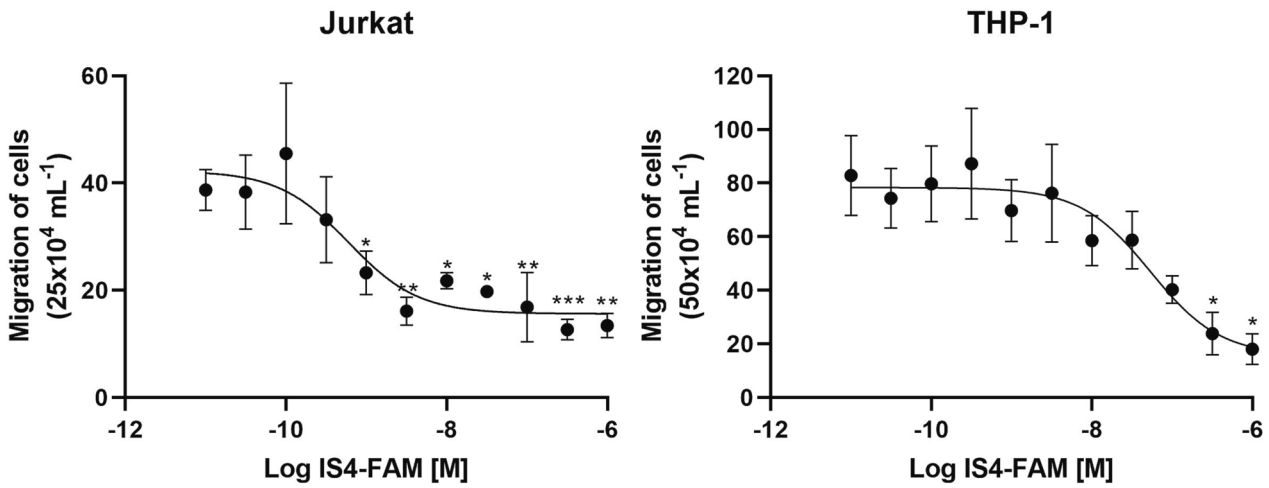

Fig. 10. IS4-FAM inhibits CXCL12 induced migration in Jurkat and THP-1 cells. Migration of $25x10^4$ mL^{-1} Jurkat cells was induced by 1 nM of CXCL12 and challenged by half log incremental concentrations of IS4-FAM (0.01 nM to 1 μM). Migration of $50x10^4$ mL^{-1} THP-1 cells was induced by 5 nM of CXCL12 and challenged by half log incremental concentrations of IS4-FAM (0.01 nM to 1 μM). Data are mean ± SD, N = 4. All IC_{50} and pIC_{50} values obtained are shown in Table 1. Data were analysed by one-way ANOVA and post hoc Dunnett's multiple comparison test comparing IS4-FAM treatment to 1 nM (Jurkat) or 5 nM (THP-1) CXCL12, $^*p < 0.05$, $^{**}p < 0.01$ and $^{***}P < 0.01$.

Table 1
Effect of four CXCR4 antagonists upon CXCL12 induced migration in Jurkat and THP-1 cell lines. Equation = Log (Inhibitor) vs. response – Variable slope (four parameters) Hill Slope = 1. Data representative of the mean SD ± of 4 independent experiments.

Jurkat cells				
All antagonists in the presence of 1 nM CXCL12				
Parameters	**AMD3100**	**Peptide 10**	**IS4**	**IS4-FAM**
IC_{50}	18.22 nM	0.56 nM	38.75 nM	0.60 nM
pIC_{50} ± SE	7.74 ± 0.37	9.26 ± 0.42	7.41 ± 0.42	9.22 ± 0.34
THP-1 cells				
All antagonists in the presence of 5 nM CXCL12				
Parameters	**AMD3100**	**Peptide 10**	**IS4**	**IS4-FAM**
IC_{50}	70.05 nM	0.12 nM	0.65 nM	53.63 nM
pIC_{50} ± SE	7.16 ± 0.39	9.92 ± 0.32	9.19 ± 0.44	7.27 ± 0.34

chemotaxis assays were conducted on Jurkat, and THP-1 cells pre-treated with increasing concentrations of antagonists (Fig. 10 and Table 1). All compounds exhibited antagonistic effects within the nanomolar range. Of the four tested CXCR4 antagonists, peptide 10 was the most potent; pIC_{50} values for Jurkat cells; 9.26 ± 0.42 (IC_{50} 0.56 nM) and THP-1 cells; 9.92 ± 0.32 (IC_{50} 0.12 nM). IS4-FAM was more potent than AMD3100 in both Jurkat cells; 9.22 ± 0.346 (IC_{50} 0.60 nM) and 7.74 ± 0.37 (IC_{50} 18.22 nM) respectively and in THP-1 cells; 7.27 ± 0.43 (IC_{50} 53.63 nM) and 7.16 ± 0.39 (IC_{50} 70.05 nM), respectively.

3.5. IS4 and IS4-FAM inhibits CXCL12-induced migration in adherent cells (PC3 and SK-MEL-28)

To evaluate the capacity of the CXCR4 antagonists to compete with CXCL12 in adherent cells, time-lapse assays were conducted on PC3, and SK-MEL-28 cells pre-treated with 1 μM of CXCR4 antagonists (Fig. 11A-B and Table 2). While AMD3100 did not exhibited any significant antagonistic effects in PC3 and SK-MEL-28 cells peptide 10, IS4 and IS4-FAM all caused a significant inhibition in cellular migration speeds. As compared to the control (10 nM CXCL12, 77.97 ± 6.11 μm/hr), basal PC3 cell migratory speeds were 37.82 ± 16.36 μm/hr which fell to 11.76 ± 7.02 μm/hr with 1 μM peptide 10, 11.76 ± 6.91 μm/hr with 1 μM IS4 and 23.25 ± 8.71 μm/hr with 1 μM IS4-FAM. In SK-MEL-28 cells, as compared to the control (10 nM CXCL12, 31.22 ± 2.22 μm/hr) basal cell migratory speeds were 10.75 ± 2.00 μm/hr which increased to 17.88 ± 1.04 μm/hr with 1 μM peptide 10 treatment, 9.33 ± 1.68 μm/hr with 1 μM IS4 and 15.99 ± 6.70 μm/hr with 1 μM IS4-FAM.

PC3 and SK-MEL-28 cells were further subjected to incremental concentration of IS4-FAM and demonstrated that IS4-FAM exhibited significant antagonistic effects as compared to the positive 10 nM CXCL12 control (Fig. 11C-D).

3.6. IS4-FAM is a competitive antagonist

In addition to the migratory assays, flow cytometry was used to investigate competition between the fluorescent IS4-FAM and the non-fluorescent IS4. First, we demonstrated the saturable binding of IS4-FAM in both Jurkat and MCF-7 which determined K_d values of 22.88 ± 8.98 μM and 4.57 ± 0.71 μM, respectively (Fig. 12A-D). When using half log incremental concentrations of IS4 (1 μM to 10 μM) in addition to 1 μM IS4-FAM, there was a visible concentration-dependent decrease in fluorescence in Jurkat cells (Fig. 12E-F). However, only high concentration of IS4 (10 μM) caused a significant decrease in fluorescence in MCF-7 cells (Fig. 12G-H). Furthermore, we could reduce IS4-FAM binding with high concentrations of IS4 in Jurkat cells whereby the K_d significantly increases from 22.88 ± 8.98 μM to 65.38 ± 12.92 μM in the presence of 3 μM IS4 and to 81.48 ± 17.74 μM in the presence of 10 μM IS4 (Fig. 12I). In MCF-7 cells, the K_d significantly increases from 4.57 ± 0.71 μM to 8.93 ± 1.59 nM in the presence of 10 μM IS4 (Fig. 12J).

3.7. IS4-FAM binds specifically to CXCR4 and does not have off-target inhibitory effects in other chemokine receptors

To determine if there were any off-target effects of IS4-FAM, $CXCR4^-$ CHO cells and Jurkat cells were treated with 1 μM IS4-FAM where it was found that minimum fluorescence was seen in the CHO cells (relative expression 1.11 ± 0.01) as compared to Jurkat cells (relative expression 29.31 ± 3.98) (Fig. 13A-C).

Additionally, chemotaxis assays were conducted whereby THP-1 cells were inhibited with 1 μM IS4 or 1 μM IS4-FAM then stimulated with 5 nM of CXCL8, CXCL10, CXCL12, CXCL13, CXCL16 and CCL5 (Fig. 13D and E). No significant inhibition was seen except for CXCL12 stimulated migration.

3.8. IS4-FAM remains stable after incubation in foetal bovine serum

As determined in Bottger at al., [49], peptides degraded the fastest in serum as compared to blood or plasma. Therefore, to determine if IS4

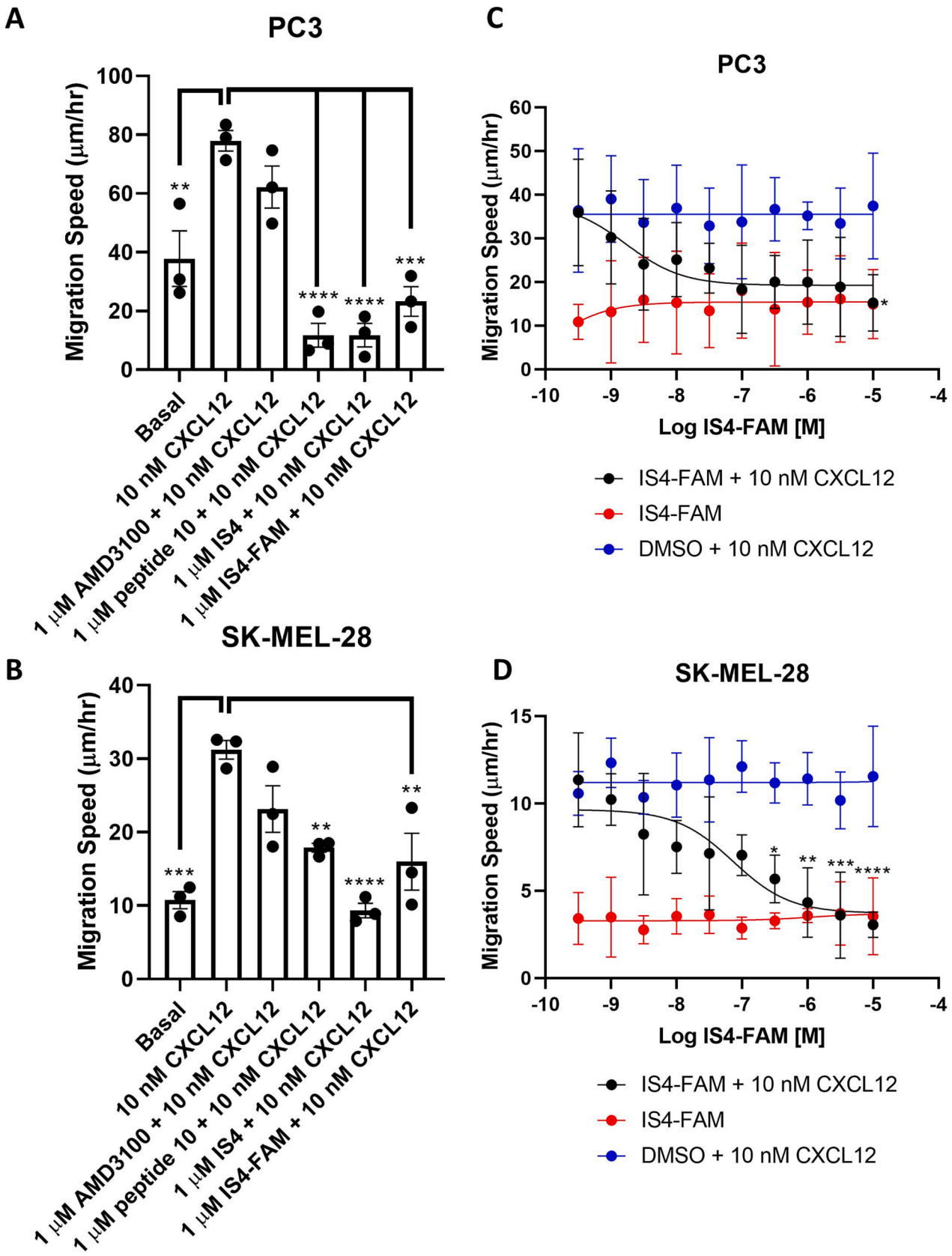

Fig. 11. Peptide 10, IS4 and IS4-FAM inhibit CXCL12 induced migration in PC3 and SK-MEL-28 cells. Migration of A) PC3 and B) SK-MEL-28 cells was induced by 10 nM of CXCL12 and challenged by 1 μM CXCR4 antagonists. Data are mean ± SD, N = 3. Migration cell speeds are shown in Table 2. Migration of C) PC3 and D) SK-MEL-28 cells was induced by 10 nM of CXCL12 and challenged by half log incremental concentrations of IS4-FAM (300 pM to 10 μM). Data are mean ± SD, N = 4. Data were analysed by one-way ANOVA and post hoc Dunnett's multiple comparison test comparing CXCR4 antagonist treatment to 10 nM CXCL12, $^{*}p < 0.05$, $^{**}p < 0.01$, $^{***}p < 0.01$ and $^{****}p < 0.001$.

Table 2
Effect of 1 μM CXCR4 antagonist upon relative cell migratory speeds as compared to 10 nM CXCL12. Data representative of the mean ± SD of 3 independent experiments. Data were analysed by one-way ANOVA and post hoc Dunnett's multiple comparison test comparing CXCR4 antagonist treatment to 10 nM CXCL12, *$p < 0.05$, **$p < 0.01$, ***$p < 0.01$ and ****$p < 0.001$.

PC3 cells	
Treatment	**Migration Speed(μm/hr)**
Basal	37.82 ± 16.36 **
10 nM CXCL12	77.97 ± 6.11
10 nM CXCL12 + 1 μM AMD3100	62.19 ± 12.45
10 nM CXCL12 + 1 μM peptide 10	11.76 ± 7.02 ****
10 nM CXCL12 + 1 μM IS4	11.76 ± 6.91 ****
10 nM CXCL12 + 1 μM IS4-FAM	423.25 ± 8.71 ***
SK-MEL-28 cells	
Treatment	**Migration Speed(μm/hr)**
Basal	10.75 ± 2.00 ***
10 nM CXCL12	31.22 ± 2.19
10 nM CXCL12 + 1 μM AMD3100	23.15 ± 5.47
10 nM CXCL12 + 1 μM peptide 10	17.88 ± 1.04 **
10 nM CXCL12 + 1 μM IS4	9.33 ± 1.68 ****
10 nM CXCL12 + 1 μM IS4-FAM	15.99 ± 6.70 **

and IS4-FAM had improved stability over peptide 10, the CXCR4 antagonists were incubated in foetal bovine serum (FBS) for 30 min at 37 °C before Ca^{2+} release assays were conducted (Fig. 14). From these results, it was determined that after only 30 min incubation with FBS, peptide 10 no longer inhibited Ca^{2+} release while IS4 and IS4-FAM remained stable and were still able to inhibit Ca^{2+} release in THP-1 cells.

3.9. IS4 and IS4-FAM are not cytotoxic

All cell lines were subject to 72-hours incubation with 1–100 μM of the four CXCR4 antagonists, Table 3. This data demonstrates that cytotoxicity was not observed in either our tumorigenic cell lines or the non-tumorigenic VSMC line when using experimental concentrations of any of the four CXCR4 antagonists.

4. Discussion

CXCR4 is the most commonly overexpressed chemokine receptor in cancer, leading to more aggressive tumours due to their increased metastatic potential [10–19]. Owing to this, CXCR4 antagonists have gained considerable interest therapeutically however, there has been

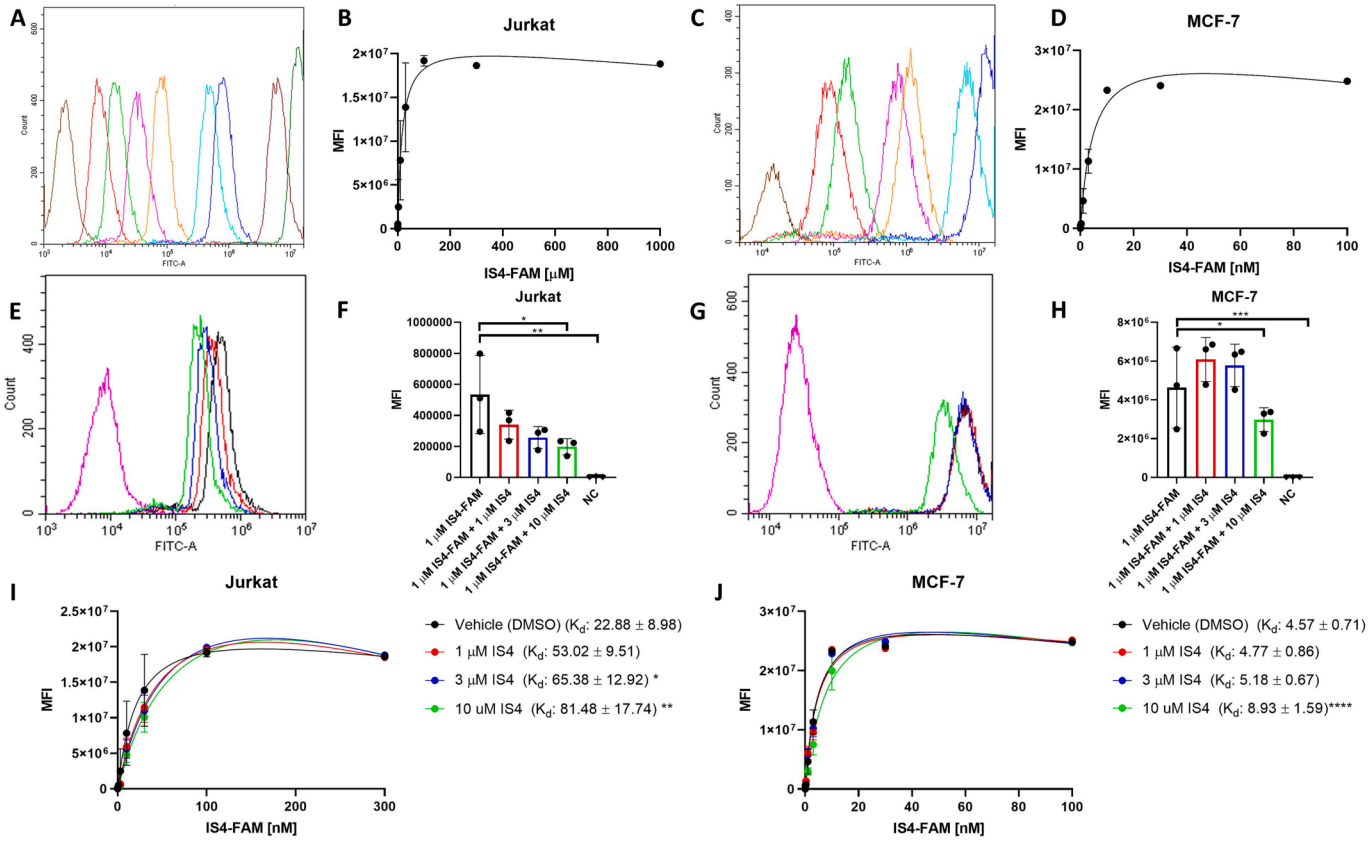

Fig. 12. Saturation and displacement binding of IS4-FAM in Jurkat and MCF-7 cells. A) Representative histogram of Jurkat cells with no CXCR4 antagonists (brown), 10 nM IS4-FAM (red), 30 nM IS4-FAM (green), 100 nM IS4-FAM (pink), 300 nM IS4-FAM (orange), 1 μM IS4-FAM (turquoise), 3 μM IS4-FAM (blue), 10 μM IS4-FAM (dark brown) and 30 μM IS4-FAM (dark green). B) Saturation binding of Jurkat cells with half log concentrations of IS4-FAM (30 nM to 1 mM). Jurkat B_{max} and K_d were 25947754.28 ± 4439438.16 and 22.88 ± 8.88 μM, respectively using one site – total saturation curve. C) Representative histogram of MCF-7 cells with no CXCR4 antagonists (brown), 10 nM IS4-FAM (red), 30 nM IS4-FAM (green), 100 nM IS4-FAM (pink), 300 nM IS4-FAM (orange), 1 μM IS4-FAM (turquoise) and 3 μM IS4-FAM (blue). D) Saturation binding of MCF-7 cells with half log concentrations of IS4-FAM (10 nM to 100 μM). MCF-7 B_{max} and K_d were 31949608.82 ± 1832727.03 and 4.57 ± 0.71 μM, respectively using one site – total saturation curve. E) Representative histogram of Jurkat cells with no CXCR4 antagonists (pink), 1 μM IS4-FAM (black), 1 μM IS4-FAM + 1 μM IS4 (red), 1 μM IS4-FAM + 3 μM IS4 (blue) and 1 μM IS4-FAM + 10 μM IS4 (green) with associated graphical representation shown in F). G) Representative histogram of MCF-7 cells with no CXCR4 antagonists (pink), 1 μM IS4-FAM (black), 1 μM IS4-FAM + 1 μM IS4 (red), 1 μM IS4-FAM + 3 μM IS4 (blue) and 1 μM IS4-FAM + 10 μM IS4 (green) with associated graphical representation shown in H). Fluorescent intensity values were measured with a blue 488 nm laser, FITC channel using FITC median fluorescence area (MFI). Data are mean ± SD, N = 3. Data were analysed by one-way ANOVA and post hoc Dunnett's multiple comparison test comparing CXCR4 antagonist treatment to 1 μM IS4-FAM. IS4-FAM displacement occurred using vehicle or 1–10 μM IS4 in I) Jurkat and J) MCF-7 cells. Data are mean ± SD, N = 3. Data were analysed by two-way ANOVA with IS4 as the between measures variable followed by Dunnett post hoc test comparing IS4 concentration to vehicle. *$p < 0.05$, **$p < 0.01$, ***$p < 0.001$ and ****$p < 0.0001$.

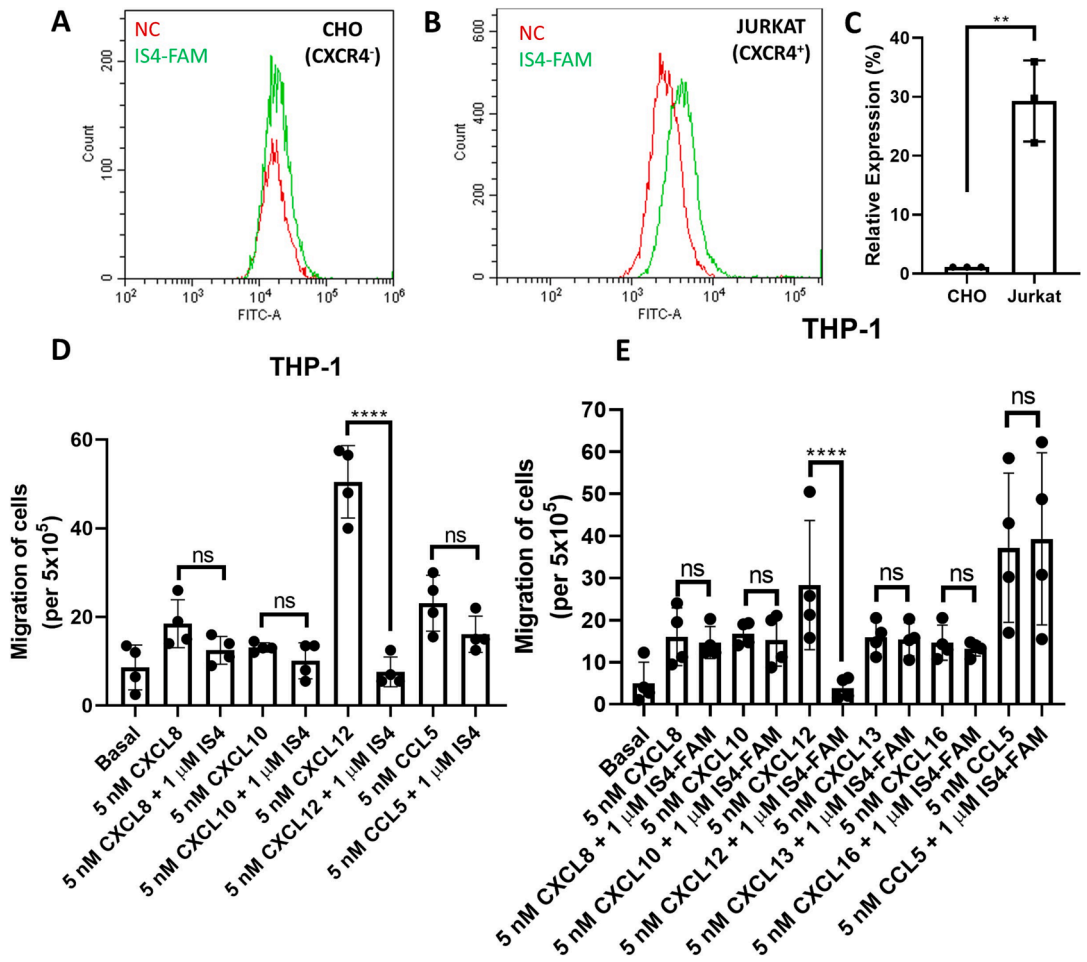

Fig. 13. IS4-FAM binds specifically to CXCR4 and does not cause off-target inhibition. Representative histograms of A) CHO (CXCR4-) cells and B) Jurkat (CXCR4 +) cells incubated with 1 μM IS4-FAM for 1 h. C) Relative expression of CXCR4 expression in CHO and Jurkat cells. Relative CXCR4 expression calculated as median fluorescence intensity of positive control (cells incubated with 1 μM IS4-FAM / median fluorescence intensity of negative control (cells only). Values acquired using CytExpert v2.4 (Beckman Coulter). Data are mean ± SD, N = 3 and analysed by two-tailed, unpaired *t*-test. Migration of THP-1 cells was induced by 5 nM of CXCL8, CXCL10, CXCL12, CXCL13, CXCL16 and CCL5 and inhibited with D) 1 μM IS4 or E) 1 μM IS4-FAM for 4 h. Data are mean ± SD, N = 4. Data were analysed by one-way ANOVA and post hoc Tukey's multiple comparison test, ns, not significant and ****$p < 0.001$.

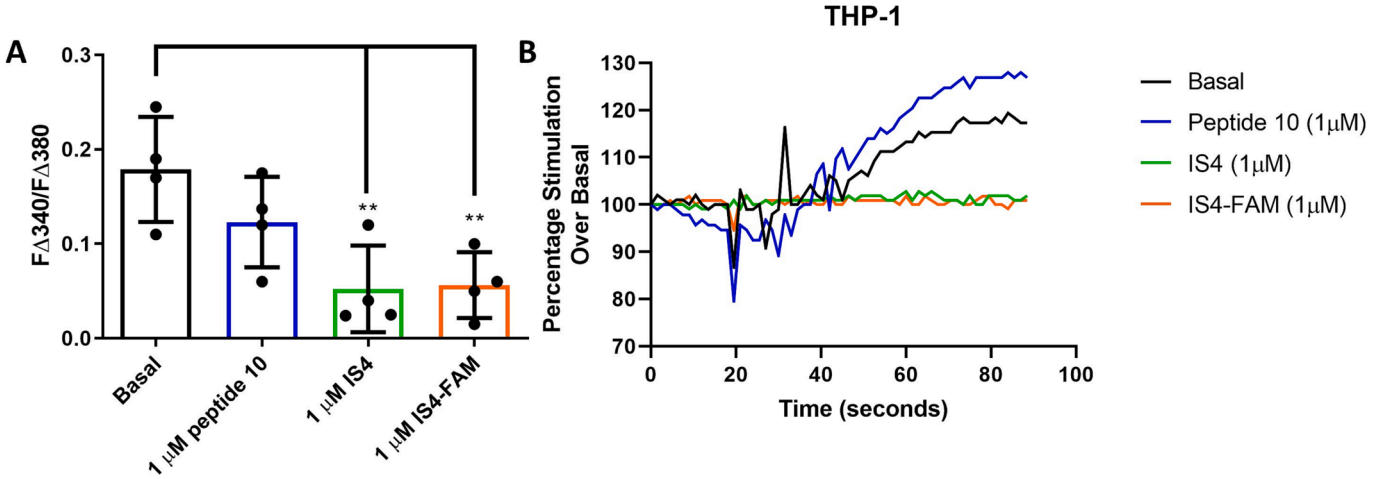

Fig. 14. IS4 and IS4-FAM remained stable after 30 min incubated in FBS. A) CXCR4 antagonists were incubated in FBS for 30 min at 37 °C. THP-1 cells were then incubated with FBS-treated CXCR4 antagonists for 30 min at 37 °C before being stimulated with 15 nM CXCL12. B) Representative intracellular calcium release trace of THP-1 cells incubated with FBS-treated CXCR4 antagonists then stimulated with 15 nM CXCL12. Data is expressed as a change in fluorescence ratio (340 nm/380 nm) where the basal fluorescence prior to the addition of CXCL12 is subtracted from peak fluorescence following the addition of CXCL12. Chemokine injected after 15 s. Data are mean ± SD N = 4. Data were analysed using one-way ANOVA with post hoc Dunnett's multiple comparison comparing basal to CXCR4 antagonist, **$P < 0.01$.

Table 3
P-values representing the non-cytotoxic effect of AMD3100, peptide 10, IS4 and IS4-FAM in five tumorigenic and one non-tumorigenic cell lines. Data representative of the mean ± SD of 3 independent experiments. Data were analysed using one-way ANOVA with post hoc Dunnett's multiple comparison comparing CXCR4 antagonist treatment to positive control (DMSO vehicle equivalent), ns not significant.

CXCR4 Antagonist	MCF-7	PC3	SK-MEL-28	Jurkat	THP-1	VSMC
1 μM AMD3100	0.95 ns	0.13 ns	0.98 ns	0.75 ns	0.99 ns	0.86 ns
1 μM peptide 10	0.98 ns	0.98 ns	>0.99 ns	>0.99 ns	0.99 ns	>0.99 ns
1 μM IS4	0.20 ns	0.85 ns	0.95 ns	>0.99 ns	0.80 ns	>0.99 ns
1 μM IS4-FAM	0.99 ns	>0.99 ns	0.99 ns	0.93 ns	0.58 ns	> 0.89 ns
100 μM IS4-FAM	>0.99 ns	>0.99 ns	0.28 ns	0.56 ns	0.98 ns	0.16 ns

little progression from pre-clinical trials [21].

In this study we compared two literature antagonists (AMD3100 and peptide 10) to our novel CXCR4 antagonist IS4. Secondly, we also demonstrate how this platform can be derivatized using CuAAC to give a fluorescent bifunctional molecule, IS4-FAM.

To confirm that IS4 was a CXCL12 mimetic, two CXCR4 mAbs were utilized; 12G5 and 4G10. The conformation-dependent mAb 12G5 recognizes determinants in ECL1 and ECL2 of CXCR4 like that of CXCL12-CXCR4 binding [31,33,36]. Hence, 12G5 and CXCL12 have been found to competitively bind CXCR4 [34–36]. Therefore, when using 1 μM of CXCR4 antagonist plus the CXCL12-othosteric mAb 12G5, no fluorescence was observed due to the antagonists already being bound to the antibodies binding site. However, when using 1 μM of CXCR4 antagonist plus the CXCL12-allosteric mAb 4G10, fluorescence could be observed, demonstrating that IS4 binding to CXCR4 is like that of the CXCL12 mimetic compounds AMD3100 and peptide 10 (Fig. 6). Furthermore, we determined that IS4-FAM specifically labels CXCR4 with minimum off-target binding as compared to the CXCR4- CHO cell line and the use of other chemokines (Fig. 13) and that our novel CXCR4 antagonist did not induce receptor internalization (Fig. 7).

IS4 and IS4-FAM can inhibit both CXCL12 stimulated intracellular calcium release (Fig. 9) and CXCL12 stimulated cellular migration in a broad spectrum of CXCR4 expressing cell lines (Figs. 10 and 11). Notably, it was determined that IS4-FAM elicits antagonistic effects upon Jurkat cells (IC_{50}: 0.60 nM) before it fully saturates the CXCR4 receptors (K_d: 22.88 ± 8.98 μM) (Fig. 12). This is likely due to the relative expression of Jurkat cells (162.70 ± 2.77) being much greater than other cell lines (Fig. 5). Indeed, MCF-7 cells (relative expression of CXCR4: 11.35 ± 0.32) had a lower K_d of 4.57 ± 0.71 μM (Fig. 5 and Fig. 12). Additionally, when comparing the two suspension cell lines, Jurkat and THP-1 cells, it can be observed that Jurkat cells homogenously express CXCR4 while THP-1 cells expression of CXCR4 is heterogeneous and have a reduced relative expression of CXCR4 (27.02 ± 3.06) (Fig. 5). Hence, THP-1 cells required a higher concentration of CXCL12 to obtain sufficient cellular migration; 1 nM CXCL12 for the Jurkat cell line vs 5 nM for THP-1 cells (Fig. 10) as well as requiring higher concentrations of CXCR4 antagonist to achieve inhibition (Table 1). This therefore determines that the greater the expression of CXCR4 on the cancer cell line, the greater the potency of the CXCR4 antagonist.

While the novel CXCR4 antagonists are more potent than AMD3100 with potency not being lost with the addition of the FAM fluorescent dye, peptide 10 was the most potent compound (Table 1). However, one of the major limitations for using peptides is that they are instable in biological environments including in serum and plasma due to the presence of proteases [50]. Di Maro et al., [24] determined that peptide 10 was stable in human plasma for up to 3 h however, in a paper by Böttger et al., [49] it was determined that generally peptides degraded the fastest in serum vs. plasma and were in fact the most stable in blood. Certainly, in our proof-of-principle experiments we determined that after 30 min in FBS at 37 °C, peptide 10 had lost its antagonistic function and could no longer inhibit CXCL12-induced calcium release in THP-1 cells (Fig. 14). By using an alternative cyclization strategy (N-prop-argyl-2,3-dibromomaleimide) the IS4 compounds maintained nanomolar inhibitory potency and showed enhanced stability in FBS (Fig. 14) [51,52]. Therefore, this data demonstrates the potential for these novel compounds to be considered for intravenous use due to their increased stability in the presence of proteases induced by the alternative cyclisation strategy. However, for consideration for oral administration further investigation of their stability under acidic conditions would be imperative. Furthermore, these synthetic changes did not introduce any cellular toxicity (Table 3) and allowed the introduction in IS4 of a synthetic handle for further derivatization through CuAAC click chemistry, as verified by the introduction of the fluorescent label in IS4-FAM (Fig. 7).

Overall, this highlights the potential of IS4 as a novel therapeutic for targeting cancer metastasis or as an investigative scientific tool. Additionally, through clicking IS4 to the FAM fluorescent dye, we have demonstrated the applicability of utilizing click chemistry to attach non-peptidic moieties to CXCR4 antagonists whilst maintaining antagonist potency and not causing cellular toxicity.

Declaration of Competing Interest

The authors declare that they have no known competing financial interests or personal relationships that could have appeared to influence the work reported in this paper.

Data availability

Data will be made available on request.

Acknowledgement

We are indebted to Dr Derek Warren at the University of East Anglia for use of his VSMCs and Alice Bradford for her assistance in the growth of these cells. We also thank James McColl at the Henry Wellcome Laboratory for Cellular Imaging for the training and assistance provided regarding microscopy image acquisition.

Funding

This research did not receive any specific grant from funding agencies in the public, commercial, or not-for-profit sectors.

Author contributions

I.H undertook the experimental work, analysed data and wrote the manuscript. M. M. D.C synthesized all the CXCR4 antagonists and edited the manuscript. W.Y.L undertook experimental work. M.S and A.M co-conceived the project and edited the manuscript.

References

[1] R.L. Siegel, K.D. Miller, N.S. Wagle, A. Jemal, Cancer statistics, 2023, CA: a cancer journal for clinicians 73(1) (2023) 17-48.
[2] H. Sung, J. Ferlay, R.L. Siegel, M. Laversanne, I. Soerjomataram, A. Jemal, F. Bray, Global cancer statistics 2020: GLOBOCAN estimates of incidence and mortality worldwide for 36 cancers in 185 countries, CA Cancer J. Clin. 71 (3) (2021) 209–249.
[3] H. Dillekås, M.S. Rogers, O. Straume, Are 90% of deaths from cancer caused by metastases? Cancer Med. 8 (12) (2019) 5574–5576.
[4] C.L. Chaffer, R.A. Weinberg, A Perspective on Cancer Cell Metastasis, Science 331 (6024) (2011) 1559–1564.

[5] P.J. Sarvaiya, D. Guo, I. Ulasov, P. Gabikian, M.S. Lesniak, Chemokines in tumor progression and metastasis, Oncotarget 4 (12) (2013) 2171.
[6] K.J. Laing, C.J. Secombes, Chemokines, Dev. Comp. Immunol. 28 (5) (2004) 443–460.
[7] B.A. Teicher, S.P. Fricker, CXCL12 (SDF-1)/CXCR4 pathway in cancer, Clin. Cancer Res. 16 (11) (2010) 2927–2931.
[8] W.Y. Lai, A. Mueller, Latest update on chemokine receptors as therapeutic targets, Biochem. Soc. Trans. 49 (3) (2021) 1385–1395.
[9] K.J. Eash, J.M. Means, D.W. White, D.C. Link, CXCR4 is a key regulator of neutrophil release from the bone marrow under basal and stress granulopoiesis conditions, Blood 113 (19) (2009) 4711–4719.
[10] M.G. Borrello, L. Alberti, A. Fischer, D. Degl'Innocenti, C. Ferrario, M. Gariboldi, F. Marchesi, P. Allavena, A. Greco, P. Collini, Induction of a proinflammatory program in normal human thyrocytes by the RET/PTC1 oncogene, Proceedings of the National Academy of Sciences of the United States of America 102(41) (2005) 14825-14830.
[11] T. Koshiba, R. Hosotani, Y. Miyamoto, J. Ida, S. Tsuji, S. Nakajima, M. Kawaguchi, H. Kobayashi, R. Doi, T. Hori, Expression of stromal cell-derived factor 1 and CXCR4 ligand receptor system in pancreatic cancer: a possible role for tumor progression, Clin. Cancer Res. 6 (9) (2000) 3530–3535.
[12] S. Mehta, K. Christopherson, P. Bhat-Nakshatri, R. Goulet, H. Broxmeyer, L. Kopelovich, H. Nakshatri, Negative regulation of chemokine receptor CXCR4 by tumor suppressor p53 in breast cancer cells: implications of p53 mutation or isoform expression on breast cancer cell invasion, Oncogene 26 (23) (2007) 3329–3337.
[13] A. Müller, B. Homey, H. Soto, N. Ge, D. Catron, M.E. Buchanan, T. McClanahan, E. Murphy, W. Yuan, S.N. Wagner, Involvement of chemokine receptors in breast cancer metastasis, Nature 410 (6824) (2001) 50–56.
[14] C.J. Scotton, J.L. Wilson, D. Milliken, G. Stamp, F.R. Balkwill, Epithelial cancer cell migration, Cancer Res. 61 (13) (2001) 4961–4965.
[15] S. Singh, U.P. Singh, W.E. Grizzle, J.W. Lillard, CXCL12–CXCR4 interactions modulate prostate cancer cell migration, metalloproteinase expression and invasion, Lab. Invest. 84 (12) (2004) 1666–1676.
[16] P. Staller, J. Sulitkova, J. Lisztwan, H. Moch, E.J. Oakeley, W. Krek, Chemokine receptor CXCR4 downregulated by von Hippel-Lindau tumour suppressor pVHL, Nature 425 (6955) (2003) 307–311.
[17] M. Vela, M. Aris, M. Llorente, J.A. Garcia-Sanz, L. Kremer, Chemokine receptor-specific antibodies in cancer immunotherapy: achievements and challenges, Front. Immunol. 6 (2015) 12.
[18] E. Phattarataratip, K. Dhanuthai, Expression of CXC motif chemokine receptors 4 and 7 in salivary gland neoplasms, Arch. Oral Biol. 83 (2017) 136–144.
[19] Z. Johnson, C. Power, C. Weiss, F. Rintelen, H. Ji, T. Ruckle, M. Camps, T. Wells, M. Schwarz, A. Proudfoot, Chemokine inhibition–why, when, where, which and how?, Biochemical Society (2004).
[20] J.F. DiPersio, E.A. Stadtmauer, A. Nademanee, I.N. Micallef, P.J. Stiff, J. L. Kaufman, R.T. Maziarz, C. Hosing, S. Früehauf, M. Horwitz, Plerixafor and G-CSF versus placebo and G-CSF to mobilize hematopoietic stem cells for autologous stem cell transplantation in patients with multiple myeloma, Blood 113 (23) (2009) 5720–5726.
[21] R. Zhao, J. Liu, Z. Li, W. Zhang, F. Wang, B. Zhang, Recent Advances in CXCL12/CXCR4 Antagonists and Nano-Based Drug Delivery Systems for Cancer Therapy, Pharmaceutics 14 (8) (2022) 1541.
[22] A.E. Proudfoot, C.A. Power, M.K. Schwarz, Anti-chemokine small molecule drugs: a promising future? Expert Opin. Invest. Drugs 19 (3) (2010) 345–355.
[23] L. Portella, R. Vitale, S. De Luca, C. D'Alterio, C. Ierano, M. Napolitano, A. Riccio, M.N. Polimeno, L. Monfregola, A. Barbieri, Preclinical development of a novel class of CXCR4 antagonist impairing solid tumors growth and metastases, PLoS One 8 (9) (2013) e74548.
[24] S. Di Maro, A.M. Trotta, D. Brancaccio, F.S. Di Leva, V. La Pietra, C. Ierano, M. Napolitano, L. Portella, C. D'Alterio, R.A. Siciliano, Exploring the N-terminal region of CXC motif chemokine 12 (CXCL12): Identification of plasma-stable cyclic peptides as novel, potent CXC chemokine receptor type 4 (CXCR4) antagonists, J. Med. Chem. 59 (18) (2016) 8369–8380.
[25] C.M. Grison, G.M. Burslem, J.A. Miles, L.K. Pilsl, D.J. Yeo, Z. Imani, S.L. Warriner, M.E. Webb, A.J. Wilson, Double quick, double click reversible peptide "stapling", Chem. Sci. 8 (7) (2017) 5166–5171.
[26] V. Hong, N.F. Steinmetz, M. Manchester, M. Finn, Labeling live cells by copper-catalyzed alkyne– azide click chemistry, Bioconjug. Chem. 21 (10) (2010) 1912–1916.
[27] C.D. Hein, X.-M. Liu, D. Wang, Click chemistry, a powerful tool for pharmaceutical sciences, Pharm. Res. 25 (2008) 2216–2230.
[28] K. Li, L.A. Lee, X. Lu, Q. Wang, Fluorogenic "click" reaction for labeling and detection of DNA in proliferating cells, Biotechniques 49 (1) (2010) 525–527.
[29] K. Sivakumar, F. Xie, B.M. Cash, S. Long, H.N. Barnhill, Q. Wang, A fluorogenic 1, 3-dipolar cycloaddition reaction of 3-azidocoumarins and acetylenes, Org. Lett. 6 (24) (2004) 4603–4606.
[30] S. Ahmed, R. Johnson, R. Solanki, T. Afewerki, F. Wostear, D. Warren, Using polyacrylamide hydrogels to model physiological aortic stiffness reveals that microtubules are critical regulators of isolated smooth muscle cell morphology and contractility, Front. Pharmacol. 13 (2022) 148.
[31] F. Baribaud, T.G. Edwards, M. Sharron, A. Brelot, N. Heveker, K. Price, F. Mortari, M. Alizon, M. Tsang, R.W. Doms, Antigenically distinct conformations of CXCR4, J. Virol. 75 (19) (2001) 8957–8967.
[32] X. Xiao, D. Norwood, Y.-R. Feng, M. Moriuchi, A. Jones-Trower, T.S. Stantchev, H. Moriuchi, C.C. Broder, D.S. Dimitrov, Inefficient Formation of a Complex among CXCR4, CD4 and gp120 in U937 Clones Resistant to X4 gp120–gp41-Mediated Fusion, Exp. Mol. Pathol. 68 (3) (2000) 139–146.
[33] B.S. Stephens, T. Ngo, I. Kufareva, T.M. Handel, Functional anatomy of the full-length CXCR4-CXCL12 complex systematically dissected by quantitative model-guided mutagenesis, Sci. Signal. 13 (640) (2020) eaay5024.
[34] G. Chen, W. Wang, S. Meng, L. Zhang, W. Wang, Z. Jiang, M. Yu, Q. Cui, M. Li, CXC chemokine CXCL12 and its receptor CXCR4 in tree shrews (Tupaia belangeri): structure, expression and function, PLoS One 9 (5) (2014) e98231.
[35] L. Pawig, C. Klasen, C. Weber, J. Bernhagen, H. Noels, Diversity and inter-connections in the CXCR4 chemokine receptor/ligand family: molecular perspectives, Front. Immunol. 6 (2015).
[36] N. Zhou, Z. Luo, J. Luo, D. Liu, J.W. Hall, R.J. Pomerantz, Z. Huang, Structural and functional characterization of human CXCR4 as a chemokine receptor and HIV-1 co-receptor by mutagenesis and molecular modeling studies, J. Biol. Chem. 276 (46) (2001) 42826–42833.
[37] X. Carnec, L. Quan, W.C. Olson, U. Hazan, T. Dragic, Anti-CXCR4 monoclonal antibodies recognizing overlapping epitopes differ significantly in their ability to inhibit entry of human immunodeficiency virus type 1, J. Virol. 79 (3) (2005) 1930–1933.
[38] E. De Clercq, N. Yamamoto, R. Pauwels, M. Baba, D. Schols, H. Nakashima, J. Balzarini, Z. Debyser, B.A. Murrer, D. Schwartz, Potent and selective inhibition of human immunodeficiency virus (HIV)-1 and HIV-2 replication by a class of bicyclams interacting with a viral uncoating event, Proceedings of the National Academy of Sciences 89(12) (1992) 5286-5290.
[39] E. De Clercq, N. Yamamoto, R. Pauwels, J. Balzarini, M. Witvrouw, K. De Vreese, Z. Debyser, B. Rosenwirth, P. Peichl, R. Datema, Highly potent and selective inhibition of human immunodeficiency virus by the bicyclam derivative JM3100, Antimicrob. Agents Chemother. 38 (4) (1994) 668–674.
[40] S. Hatse, K. Princen, L.-O. Gerlach, G. Bridger, G. Henson, E. De Clercq, T. W. Schwartz, D. Schols, Mutation of Asp171 and Asp262 of the chemokine receptor CXCR4 impairs its coreceptor function for human immunodeficiency virus-1 entry and abrogates the antagonistic activity of AMD3100, Mol. Pharmacol. 60 (1) (2001) 164–173.
[41] M.M. Rosenkilde, L.-O. Gerlach, J.S. Jakobsen, R.T. Skerlj, G.J. Bridger, T. W. Schwartz, Molecular mechanism of AMD3100 antagonism in the CXCR4 receptor: transfer of binding site to the CXCR3 receptor, J. Biol. Chem. 279 (4) (2004) 3033–3041.
[42] S.P. Fricker, V. Anastassov, J. Cox, M.C. Darkes, O. Grujic, S.R. Idzan, J. Labrecque, G. Lau, R.M. Mosi, K.L. Nelson, Characterization of the molecular pharmacology of AMD3100: a specific antagonist of the G-protein coupled chemokine receptor, CXCR4, Biochem. Pharmacol. 72 (5) (2006) 588–596.
[43] J.C. Knight, A.J. Hallett, A. Brancale, S.J. Paisey, R.W. Clarkson, P.G. Edwards, Evaluation of a fluorescent derivative of AMD3100 and its interaction with the CXCR4 chemokine receptor, Chembiochem 12 (17) (2011) 2692–2698.
[44] M.J. Endres, P.R. Clapham, M. Marsh, M. Ahuja, J.D. Turner, A. McKnight, J. F. Thomas, B. Stoebenau-Haggarty, S. Choe, P.J. Vance, CD4-independent infection by HIV-2 is mediated by fusin/CXCR4, Cell 87 (4) (1996) 745–756.
[45] A. Brelot, N. Heveker, O. Pleskoff, N. Sol, M. Alizon, Role of the first and third extracellular domains of CXCR-4 in human immunodeficiency virus coreceptor activity, J. Virol. 71 (6) (1997) 4744–4751.
[46] D.J. Chabot, P.-F. Zhang, G.V. Quinnan, C.C. Broder, Mutagenesis of CXCR4 identifies important domains for human immunodeficiency virus type 1 X4 isolate envelope-mediated membrane fusion and virus entry and reveals cryptic coreceptor activity for R5 isolates, J. Virol. 73 (8) (1999) 6598–6609.
[47] I. Mertens, A. Vandingenen, T. Meeusen, A. De Loof, L. Schoofs, Postgenomic characterization of G-protein-coupled receptors, Pharmacogenomics 5 (6) (2004) 657–672.
[48] R.J. Lefkowitz, Historical review: a brief history and personal retrospective of seven-transmembrane receptors, Trends Pharmacol. Sci. 25 (8) (2004) 413–422.
[49] R. Böttger, R. Hoffmann, D. Knappe, Differential stability of therapeutic peptides with different proteolytic cleavage sites in blood, plasma and serum, PLoS One 12 (6) (2017) e0178943.
[50] D.P. McGregor, Discovering and improving novel peptide therapeutics, Curr. Opin. Pharmacol. 8 (5) (2008) 616–619.
[51] M.W. Jones, R.A. Strickland, F.F. Schumacher, S. Caddick, J.R. Baker, M.I. Gibson, D.M. Haddleton, Polymeric dibromomaleimides as extremely efficient disulfide bridging bioconjugation and pegylation agents, J. Am. Chem. Soc. 134 (3) (2012) 1847–1852.
[52] H.C. Kolb, M. Finn, K.B. Sharpless, Click chemistry: diverse chemical function from a few good reactions, Angew. Chem. Int. Ed. 40 (11) (2001) 2004–2021.